

peptides and glycopeptides, and then both the peptide and sugar chain of each glycopeptide must be analyzed. One of the most effective techniques for mapping proteolytic fragments of glycoproteins is liquid chromatography (LC) coupled with electrospray ionization (ESI) mass spectrometry (MS) (Carr *et al.*, 1993; Duffin *et al.*, 1992; Kawasaki *et al.*, 2004; Ling *et al.*, 1991). The specific detection of glycopeptides can be achieved by monitoring specific diagnostic sugar oxonium ions, such as  $m/z$  204 (HexNAc) and 366 (HexHexNAc) produced by cone voltage fragmentation, or by precursor ion scanning (Carr *et al.*, 1993; Duffin *et al.*, 1992). However, when many *N*-glycosylation sites are present within a glycoprotein, the chromatogram becomes extremely complex and assignment of the glycopeptide ions is very difficult.

We present here an alternative strategy for the site-specific glycosylation analysis of a peptide and glycopeptide mixture using LC/ESI MS/MS, where we acquired the product ion spectrum for all significant molecular ions in a data-dependent manner. Product ion spectra of molecular ions allow the specific detection of glycopeptides from a complex mixture of peptides based on the presence of diagnostic sugar oxonium ions of oligosaccharides. Furthermore, this

method allows confirmation of the amino acid sequence of a glycopeptide by the presence of *b*- and *y*-series fragment ions of the peptide. Using this method, we identified one previously unidentified *N*-glycosylated site of ApoB100 and determined the oligosaccharide heterogeneity of each of 17 *N*-glycosylation sites. Our findings provide information on the structure of apoB100 that will be useful to future studies on the structure, function, and metabolism of plasma LDL.

## Results

### Enzyme digestion

To determine the oligosaccharide heterogeneity at each glycosylation site, reduced and carboxymethylated apoB100 was digested into peptides and glycopeptides. Table I shows the amino acid sequences of the tryptic or chymotryptic peptides, including the putative *N*-glycosylation sites. The putative glycosylation sites were numbered (G1–19). Boldface indicates the previously reported *N*-glycosylation sites (G2–6 and G9–19). When apoB100 is digested by trypsin, potential *N*-glycosylation sites, Asn1341 (G4) and Asn1350 (G5), belong to the same peptide. Because chymotrypsin

**Table I.** The amino acid sequences of the tryptic or chymotryptic peptides including the putative *N*-glycosylation sites in apoB100

<i>N</i> -glycosylation site <sup>a</sup>		Tryptic digests	Chymotryptic digests		
Residue	ID	Sequence	Theoretical mass <sup>b</sup>	Sequence	Theoretical mass <sup>b</sup>
Asn <sup>7</sup>	G1	EEEMLEN <sup>7</sup> VSLVCPK	1677.8	EN <sup>7</sup> VSL	560.3
Asn <sup>158</sup>	G2	QVLFLDVTYGN <sup>158</sup> CSTHFIVK	2229.1	GN <sup>158</sup> CSTHF	822.3
Asn <sup>956</sup>	G3	QVFPGLNYCTSGAYSN <sup>956</sup> ASSTDSASYPLTGDR	3550.5	SN <sup>956</sup> ASSTDSASY	1088.4
Asn <sup>1341</sup>	G4	LYQLQVPLLGVLDLSTNVYSNLYN <sup>1341</sup>	4692.3	N <sup>1341</sup> W	318.1
Asn <sup>1350</sup>	G5	WSASYSGGN <sup>1350</sup> TSTDHFSLR	4692.3	SGGN <sup>1350</sup> TSTDHF	1021.4
Asn <sup>1496</sup>	G6	FN <sup>1496</sup> SSYLQGTNQTGR	1684.8	N <sup>1496</sup> SSY	469.2
Asn <sup>2212</sup>	G7	TIHDLHLFIENIDFN <sup>2212</sup> K	1968.0	N <sup>2212</sup> KSGSSTASW	1023.5
Asn <sup>2533</sup>	G8	N <sup>2533</sup> LTDFAEQYSIQDWAK	1928.9	AAKN <sup>2533</sup> L	515.3
Asn <sup>2752</sup>	G9	IQSPLFTLDANADIGN <sup>2752</sup> GTTSANEAGIAASITAK	3231.6	DANADIGN <sup>2752</sup> GTTSANEAGIAASITAKGESKL	2846.4
Asn <sup>2955</sup>	G10	VNQNLVYESGSLN <sup>2955</sup> FSK	1797.9	N <sup>2955</sup> F	279.1
Asn <sup>3074</sup>	G11	YNQN <sup>3074</sup> FSAGNNENIMEAHVINGEANLD FLNIPLTIPEMR	4359.1	NQN <sup>3074</sup> F	521.2
Asn <sup>3197</sup>	G12	SYN <sup>3197</sup> ETK	740.3	N <sup>3197</sup> ETKIKF	878.5
Asn <sup>3309</sup>	G13	ELCTISHIFIPAMGN <sup>3309</sup> ITYDFSFK	2704.3	IPAMGN <sup>3309</sup> ITY	978.5
Asn <sup>3331</sup>	G14	SSVITLNTNAELFN <sup>3331</sup> QSDIVAHLLSSSSVIDALQYK	3864.0	N <sup>3331</sup> QSDIV AHL	995.5
Asn <sup>3384</sup>	G15	FVEGSHN <sup>3384</sup> STVSLTTK	1605.8	VEGSHN <sup>3384</sup> STVSL	1128.5
Asn <sup>3438</sup>	G16	YDFN <sup>3438</sup> SSMLYSTAK	1525.7	N <sup>3438</sup> SSML	550.2
Asn <sup>3868</sup>	G17	FEVDSPVYN <sup>3868</sup> ATWSASLK	1912.9	N <sup>3868</sup> ATW	490.2
Asn <sup>4210</sup>	G18	VHN <sup>4210</sup> GSEILFSYFQDLVITLPFELR	2836.5	SKVHN <sup>4210</sup> GSEIL	1082.6
Asn <sup>4404</sup>	G19	DFHSEYIVSASN <sup>4404</sup> FTSQLSSQVEQFLHR	3155.5	IVSASN <sup>4404</sup> F	736.4

Human apoB100 amino acid sequence (NP\_000375, apolipoprotein B [gi:4502153]) was obtained from the NCBI database ([www.ncbi.nlm.nih.gov/pubmed](http://www.ncbi.nlm.nih.gov/pubmed)). Boldface indicates previously reported *N*-glycosylation sites. Cystein residue was carboxymethylated, and carboxymethylated cystein was underscored.

<sup>a</sup>Potential *N*-glycosylation sites were identified with the consensus sequence NXS/T, where X is any amino acid except P.

<sup>b</sup>Monoisotopic mass value.

can cleave apoB100 into glycopeptides containing one glycosylation site, we attempted to analyze both proteolytic fragments from trypsin digestion and chymotrypsin digestion to identify the site-specific glycosylation.

#### LC/ESI MS/MS analysis of tryptic digest of apoB100

The schema of a site-specific glycosylation analysis of apoB100 is shown in Figure 1. A mixture of peptides and glycopeptides was subjected to LC/ESI MS/MS with a reversed-phase column. Figure 2A shows a total ion chromatogram (TIC) of a time-of-flight (TOF) MS scan for the full scan  $m/z$  1000–2000. When double or higher charged molecular ions were detected, the product ion spectrum was automatically acquired. Figure 2B shows a TIC of the product ion scan. The collision energy at the second quadrupole for the product ion scan was adjusted from 50 to 80 eV depending on the size and charge of the precursor ion. Under these conditions, peptide precursor ions produced b- and y-series fragment ions derived from its amino acid sequence (data not shown), and glycopeptide precursor ions produced abundant carbohydrate-specific ions,  $m/z$  204, 186, 168, and 366 (described later). The intensity of ions at  $m/z$  204.05–204.15 (HexNAc, 204.08) in each product ion scan are illustrated in Figure 2C. The extracted ion chromatogram at  $m/z$  204 (Figure 2C) and 366 (data not shown) provides useful information on the selection of glycopeptide precursor ions. The product ion spectra of glycopeptides show a very characteristic pattern (see later figures). There were intense oligosaccharide-derived peaks of  $m/z$  204 (HexNAc), 366 (HexHexNAc), 186 (HexNAc-H<sub>2</sub>O), and 168 (HexNAc-2H<sub>2</sub>O), and if present, 163 (Hex), 292 (Neu5Ac), and 274 (Neu5Ac-H<sub>2</sub>O). Therefore, we can very easily distinguish the glycopeptide precursor ions from peptide ions. As expected, many parent ions having 204 and

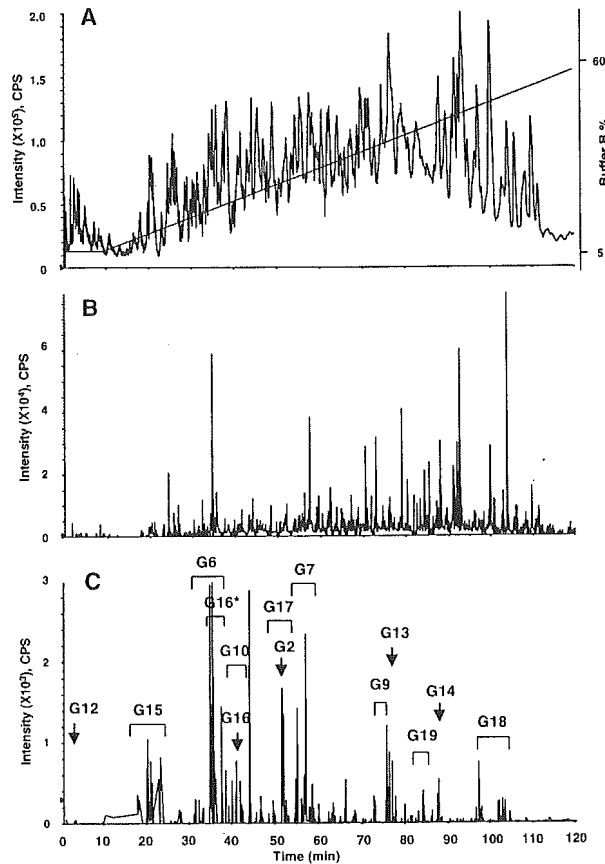


Fig. 2. LC/ESI MS/MS of tryptic digest of apolipoprotein B100. TIC of the TOF MS scan for the full scan  $m/z$  1000–2000 and the HPLC gradient are indicated (A). TIC of the product ion scan data-dependently acquired (B). Extracted ion chromatogram at  $m/z$  204 of product ion spectra (C). Arrows and brackets denote glycopeptide fraction and *N*-glycosylation site ID. G16\* was found to be oxidized at a methionine residue.

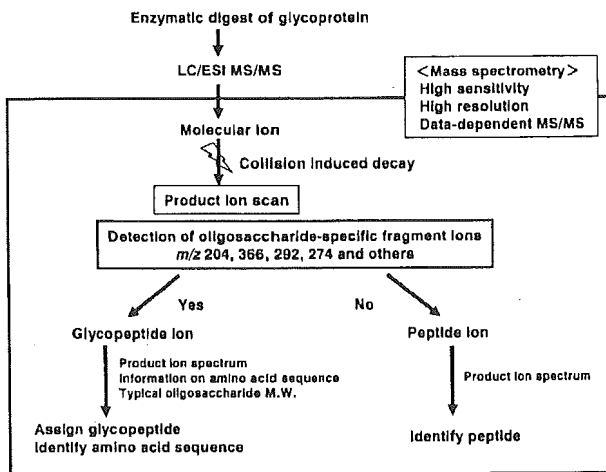


Fig. 1. Schema of site-specific glycosylation analysis. Glycoprotein was digested into peptides and glycopeptides containing only one glycosylation site. Only LC/ESI MS/MS was used. Data-dependent MS/MS acquisition was used to differentiate glycopeptide ions from peptide ions and identify the amino acid sequence of the glycopeptides. The oligosaccharide structure was deduced based on the calculated oligosaccharide molecular weight.

366 fragment ions in the product ion spectrum were detected, and most of these precursor ions were found as glycopeptides.

The glycopeptides were assigned based on an examination of product ion spectra using the information on the peptides containing a putative *N*-glycosylation site. Figures 3A, 3B, and 3C show the product ion spectra of 1412.1 (+2) at 18 min, 1160.4 (+3) at 20 min and 1271.1 (+3) at 22 min for the glycopeptides. There were intense carbohydrate B<sup>+</sup> ions such as  $m/z$  204 (HexNAc), 366 (HexHexNAc), and 186 (HexNAc-H<sub>2</sub>O) and other weak peaks in the product ion spectra. These product ion spectra were very similar to each other (Figure 3A, 3B, and 3C). Careful examination of these product ion spectra for the glycopeptides revealed that several fragment ions were consistent with b- and y-series fragment ions derived from the peptide FVEGSHNSTVSLTTK (residue 3378–3392). The deduced b- and y-series fragment ions of the peptide FVEGSHNSTVSLTTK were listed, and the fragment ions detected in the product ion spectrum of 1160.4 (+3) are underscored in the table (Figure 3D). The molecular ions of the peptide ( $m/z$  1606) and

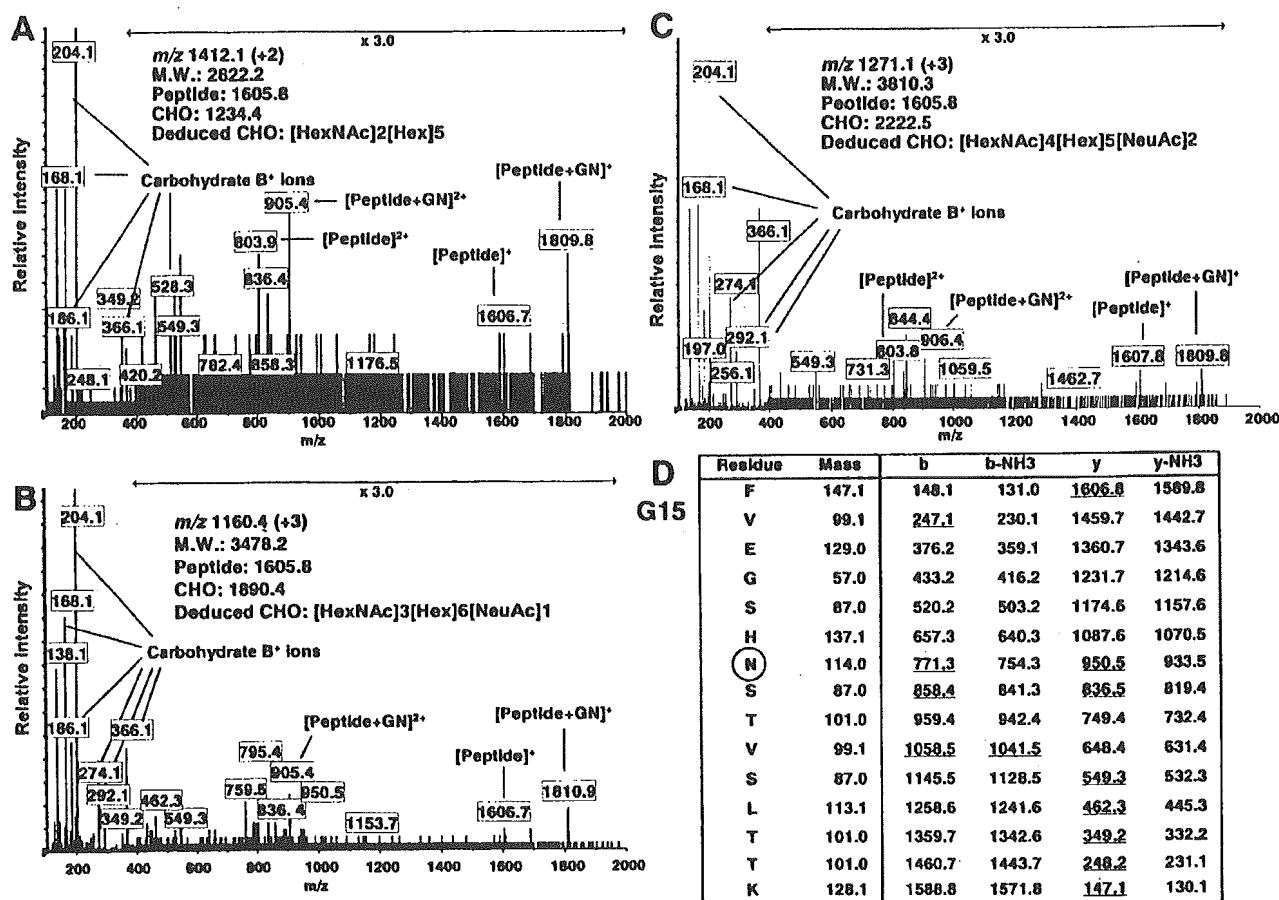


Fig. 3. Product ion spectra of the *N*-glycosylated peptides containing Asn3384 (G15). Product ion scan of  $m/z$  1412.1 (+2) (A), 1160.4 (+3) (B), and 1271.1 (+3) (C) at 18, 20, and 22 min, respectively. These spectra show a characteristic fragmentation pattern with abundant carbohydrate-diagnostic oxonium ions at 163, 168, 186, 204, and 366 and very similar patterns to each other. The oxonium ions at  $m/z$  292 (Neu5Ac) and 274 (Neu5A-H<sub>2</sub>O) were observed in the peptides having sialylated oligosaccharide (B) and (C). Several fragment ions are consistent with the b- and y-series fragment ions derived from the peptide FVEGSHNSTVSLTTK (residue 3378–3392). [Peptide]<sup>+</sup> and [peptide+GlcNAc]<sup>+</sup> ions were also detected. (D) shows  $m/z$  of the proposed b- and y-series fragment ions of the peptide and the fragment ions detected in Figure 3B are underscored. Based on the calculated oligosaccharide mass, the deduced oligosaccharide structure was presented. GN, *N*-acetylglucosamine.

peptide + GlcNAc ( $m/z$  1809) were also detected in the product ion spectra (Figure 3A, 3B, and 3C). These results suggest that these glycopeptides have the same peptide, FVEGSHNSTVSLTTK, including the *N*-glycosylation site Asn3384 (G15). Carbohydrate molecular weight was calculated by subtracting the theoretical molecular weight of the peptide (1605.8) from the calculated molecular weight of the glycopeptide and adding the molecular weight of H<sub>2</sub>O (18.0). The oligosaccharide structure was deduced based on the molecular weight and previously reported oligosaccharides of apoB100. The presence of product ions at  $m/z$  274 (Neu5Ac-H<sub>2</sub>O) and 292 (Neu5Ac) suggested that those at  $m/z$  1160.4 (+3) and 1271.1 (+3) were glycopeptide ions having sialylated oligosaccharides. Thus the carbohydrate compositions, [HexNAc]<sub>2</sub>[Hex]<sub>5</sub>, [HexNAc]<sub>3</sub>[Hex]<sub>6</sub>[NeuAc]<sub>1</sub>, and [HexNAc]<sub>4</sub>[Hex]<sub>5</sub>[NeuAc]<sub>2</sub>, were deduced from the carbohydrate molecular weights, 1234.4, 1890.4, and 2222.5, respectively.

Figures 4 shows the product ion spectra of 1294.8 (+3) at 55 min and 1152.7 (+3) at 35 min for other glycopeptides. There are intense carbohydrate B<sup>+</sup> ions in the product ion spectra. Several ions consisting of b- and y-series fragment ions from the peptide TIHDLHLFIENIDHNK (residue 2198–2213) were found in the product ion spectrum of 1294.8 (+3) (Figure 4A), and detected ions are underscored in the table. The molecular ions of the peptide ( $m/z$  1968.9) were also detected in the product ion spectra. The carbohydrate molecular weight was calculated from the molecular weight of the peptide, 1968.0, and the molecular weight of the glycopeptide, 3881.4. Carbohydrate composition was deduced from the carbohydrate molecular weight (1931.4) and presence of Neu5Ac. Thus, the peptide moiety TIHDLHLFIENIDHNK and carbohydrate composition [HexNAc]<sub>4</sub>[Hex]<sub>5</sub>[NeuAc]<sub>1</sub> were suggested.

Many ions in the product ion spectrum of 1152.7 (+3) were consistent with the b- and y-series fragment ions

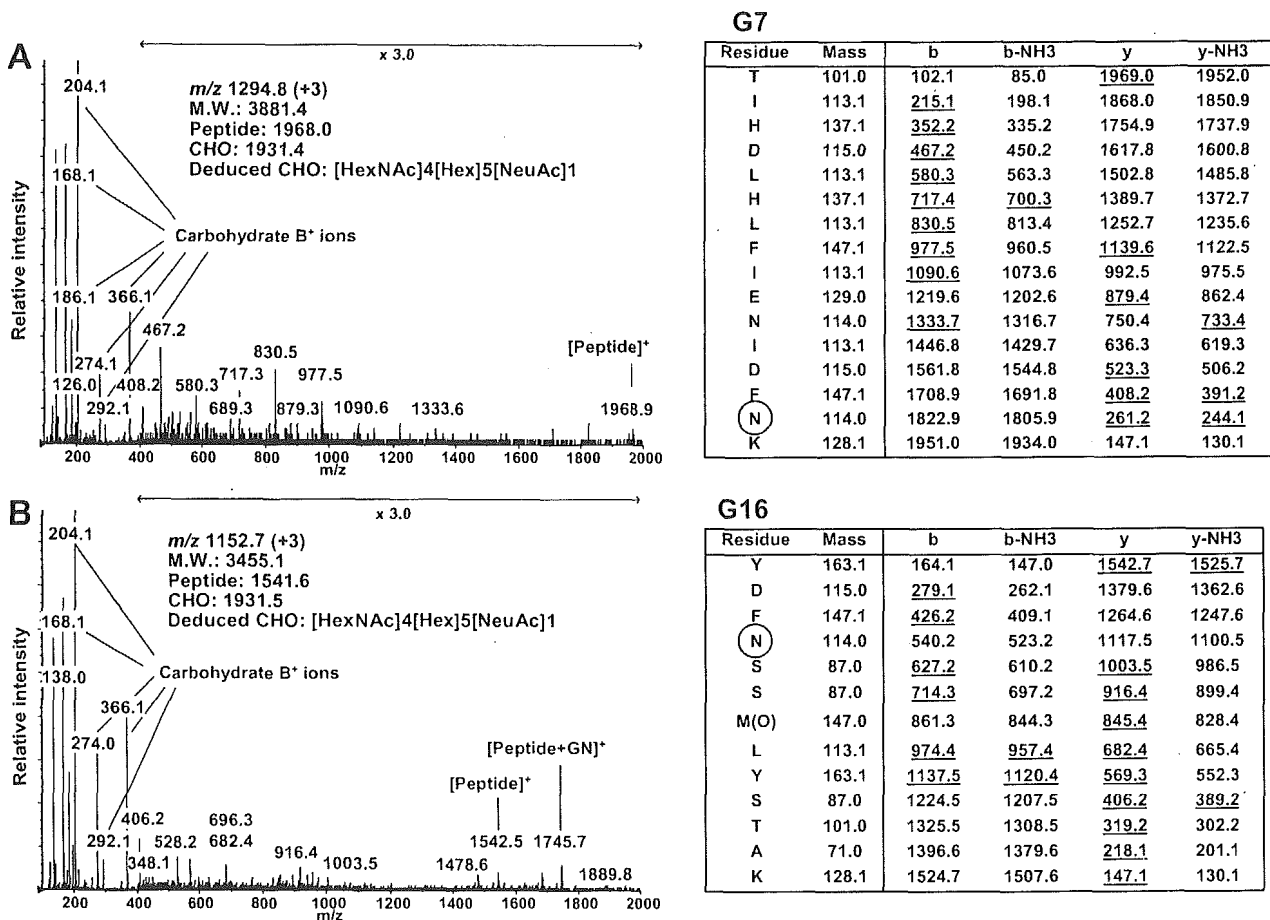


Fig. 4. Product ion spectra of the tryptic *N*-glycosylated peptides of apoB100. (A) Product ion spectrum of  $m/z$  1294.8 (+3) at 55 min for the glycopeptide containing Asn2212 (G7). Several ions are consistent with the b- and y-series fragment ions derived from the peptide TIFDLHLFIENIDFNK (residue 2198–2213). Table shows  $m/z$  of the proposed b- and y-series fragment ions and the detected ions are underscored. (B) Product ion spectrum of  $m/z$  1152.7 (+3) at 35 min for the glycopeptide containing Asn3438 (G16) with oxidized methionine. The methionine residue at 3441 was considered oxidized. Several ions are consistent with the b- and y-series fragment ions derived from the peptide YDFNSSM(O)LYSTAK (residue 3435–3447). Table shows  $m/z$  of the proposed b- and y-series fragment ions and the detected ions are underscored. M(O), oxidized methionine.

derived from the peptide YSFNSSMLYSTAK (Figure 4B). However, the deduced peptide ion  $m/z$  at 1526.7 and peptide + GlcNAc at 1729.8 were not detected. The difference of 203 between the product ions at  $m/z$  1542.5 and 1745.7 suggests that the molecular weight of the peptide moiety may be 1541.5, and an increase in mass of 16 Da suggests that the methionine residue of YSFNSSMLYSTAK (residue 3435–3447, molecular weight 1525.7) was oxidized. The deduced b- and y-series fragment ions of the peptide, YSFNSSMLYSTAK, with the oxidized methionine are listed and detected peptide fragment ions are underscored. Thus, the product ions at  $m/z$  1542.5 and 1745.7 were considered the peptide and peptide + GlcNAc ions, respectively. Our method identified unexpected oxidation of methionine residue (Figure 4B). The carbohydrate molecular weight was calculated, and the carbohydrate composition, [HexNAc]<sub>4</sub>[Hex]<sub>5</sub>[Neu5Ac]<sub>1</sub>, was deduced from the carbohydrate molecular weight, 1931.4, and presence of Neu5Ac.

Results of site-specific glycosylation analysis from tryptic digest are summarized in Table II. To avoid misassignment, only ions that were confirmed as glycopeptides by the product ion spectra or coeluting ions with glycopeptides were listed. We determined 13 of the 19 potential *N*-glycosylation sites and the oligosaccharide heterogeneity at each site in a site-specific glycosylation analysis of the tryptic digest of apoB100. The type of oligosaccharide was deduced based on the oligosaccharide composition. Glycopeptides containing *N*-glycosylation sites Asn7, 956, 1341, 1350, 2533, and 3074 (G1, 3, 4, 5, 8, and 11) could not be detected. The relative peak intensity does not accurately express the relative amount of glycoforms, because of the different ionization efficiency of each glycoform, different detection sensitivity at  $m/z$ , and simultaneous acquisition of MS and MS/MS spectra. However, the relative peak intensity of each glycopeptide would provide an indication of the distribution in glycoforms.

Table II. Site-specific glycosylation analysis of the tryptic digest of apoB100 using LC/ESI MS/MS

Glycosylation site ID	Retention time (min)	Peptide theoretical MW <sup>a</sup>	<i>m/z</i>	Glycopeptides			Oligosaccharide			Deduced Type <sup>c</sup>
				Charge	Calculated MW <sup>a</sup>	Calculated MW <sup>a</sup>	Theoretical MW <sup>a</sup>	Relative peak intensity (%) <sup>b</sup>	Composition <sup>c</sup>	
G1	—	1677.8	—	—	—	—	—	—	—	—
G2	51	2229.1	1365.6	+3	4093.8	1882.7	1882.6	7	[HexNAc]2[Hex]9	High mannose
	51	2229.1	1311.6	+3	3931.7	1720.6	1720.6	13	[HexNAc]2[Hex]8	High mannose
	51	2229.1	1257.5	+3	3769.5	1558.4	1558.5	22	[HexNAc]2[Hex]7	High mannose
	51	2229.1	1203.5	+3	3607.6	1396.6	1396.5	13	[HexNAc]2[Hex]6	High mannose
	51	2229.1	1149.5	+3	3445.5	1234.4	1234.4	100	[HexNAc]2[Hex]5	High mannose
	51	2229.1	1723.7	+2	3445.4	1234.4	—	—	—	—
G3	—	3550.5	—	—	—	—	—	—	—	—
G4, G5	—	4692.3	—	—	—	—	—	—	—	—
G6	33	1684.8	1451.6	+2	2901.2	1234.4	1234.4	15	[HexNAc]2[Hex]5	High mannose
	34	1684.8	1200.4	+3	3598.2	1931.4	1931.7	100	[HexNAc]4[Hex]5[Neu5Ac]1	Biantennary complex
	34	1684.8	1800.1	+2	3598.2	1931.4	—	—	—	—
	35	1684.8	1146.4	+3	3436.2	1769.4	1769.6	23	[HexNAc]4[Hex]4[Neu5Ac]1	Biantennary complex
	35	1684.8	1719.2	+2	3436.4	1769.6	—	—	—	—
	35	1684.8	1078.7	+3	3233.1	1566.3	1566.6	11	[HexNAc]3[Hex]4[Neu5Ac]1	Monoantennary complex
	35	1684.8	1132.8	+3	3395.4	1728.6	1728.6	5	[HexNAc]3[Hex]5[Neu5Ac]1	Hybrid
	35	1684.8	1186.8	+3	3557.4	1890.6	1890.7	3	[HexNAc]3[Hex]6[Neu5Ac]1	Hybrid
	35	1684.8	1240.8	+3	3719.4	2052.6	2052.7	3	[HexNAc]3[Hex]7[Neu5Ac]1	Hybrid
	37	1684.8	1297.4	+3	3889.2	2222.4	2222.8	24	[HexNAc]4[Hex]5[Neu5Ac]2	Biantennary complex
	37	1684.8	1945.7	+2	3889.4	2222.6	—	—	—	—
G7	54	1968.0	1294.8	+3	3881.4	1931.4	1931.7	66	[HexNAc]4[Hex]5[Neu5Ac]1	Biantennary complex
	58	1968.0	1044.2	+4	4172.8	2222.8	2222.8	100	[HexNAc]4[Hex]5[Neu5Ac]2	Biantennary complex
	58	1968.0	1391.9	+3	4172.7	2222.7	—	—	—	—
G8	—	1928.9	—	—	—	—	—	—	—	—
G9	73	3231.6	1360.4	+4	5437.6	2224.0	2222.8	—	[HexNAc]4[Hex]5[Neu5Ac]2	Biantennary complex
G10	40	1797.9	1238.1	+3	3711.3	1931.4	1931.7	41	[HexNAc]4[Hex]5[Neu5Ac]1	Biantennary complex
	41	1797.9	1856.7	+2	3711.4	1931.5	—	—	—	—

Table II. continued

Glycosylation site ID	Retention time (min)	Peptide theoretical MW <sup>a</sup>	Glycopeptides			Oligosaccharide			Relative peak intensity (%) <sup>b</sup>	Composition <sup>c</sup>	Deduced Type <sup>c</sup>
			m/z	Charge	Calculated MW <sup>a</sup>	Calculated MW <sup>a</sup>	Theoretical MW <sup>a</sup>				
G11	43	1797.9	1001.6	+4	4002.4	2222.5	2222.8	100	[HexNAc]4[Hex]5[Neu5Ac]2	Biantennary complex	
	43	1797.9	1335.1	+3	4002.3	2222.4	—	—	—	—	
	—	4339.1	—	—	—	—	—	—	—	—	
	2	740.3	1473.6	+2	2945.2	2222.9	2222.8	—	[HexNAc]4[Hex]5[Neu5Ac]2	Biantennary complex	
	75	2704.3	1102.7	+4	4406.8	1720.5	1720.6	22	[HexNAc]2[Hex]8	High mannose	
	75	2704.3	1470.0	+3	4406.9	1720.6	1558.5	54	[HexNAc]2[Hex]7	High mannose	
	76	2704.3	1062.2	+4	4244.8	1558.5	1558.5	—	—	—	
	76	2704.3	1415.9	+3	4244.7	1558.4	1558.5	—	—	—	
	76	2704.3	1021.6	+4	4082.4	1396.1	1396.5	100	[HexNAc]2[Hex]6	High mannose	
	76	2704.3	1361.9	+3	4082.7	1396.4	1396.5	—	—	—	
	76	2704.3	1307.9	+3	3920.7	1234.4	1234.4	50	[HexNAc]2[Hex]5	High mannose	
	88	3864.0	1146.7	+5	5728.7	1882.7	1882.6	—	[HexNAc]2[Hex]9	High mannose	
	88	3864.0	1433.1	+4	5728.3	1882.3	1882.3	—	—	—	
G14	17	1605.8	1063.4	+3	3187.2	1599.4	1599.6	8	[HexNAc]3[Hex]6	Hybrid	
	17	1605.8	1077.0	+3	3228.0	1640.2	1640.6	20	[HexNAc]4[Hex]5	Biantennary complex	
	17	1605.8	1009.4	+3	3025.2	1437.4	1437.5	20	[HexNAc]3[Hex]5	Hybrid	
	18	1605.8	1513.6	+2	3025.3	1437.5	1437.5	—	—	—	
	18	1605.8	1023.0	+3	3066.0	1478.2	1478.5	13	[HexNAc]4[Hex]4	Biantennary complex	
	18	1605.8	1412.1	+2	2822.2	1234.4	1234.4	4	[HexNAc]2[Hex]5	High mannose	
	20	1605.8	1174.1	+3	3519.3	1931.5	1931.7	100	[HexNAc]4[Hex]5[Neu5Ac]1	Biantennary complex	
	20	1605.8	1760.7	+2	3519.4	1931.6	1931.6	—	—	—	
	20	1605.8	1160.4	+3	3478.2	1890.4	1890.7	10	[HexNAc]3[Hex]6[Neu5Ac]1	Hybrid	
	20	1605.8	1106.4	+3	3316.2	1728.4	1728.6	94	[HexNAc]3[Hex]5[Neu5Ac]1	Hybrid	
	20	1605.8	1659.2	+2	3316.4	1728.6	1728.6	—	—	—	
	20	1605.8	1222.8	+3	3665.4	2077.6	2077.7	4	[HexNAc]4[Hex]5[Neu5Ac][Fuc]1	Biantennary complex	
	20	1605.8	1052.4	+3	3154.2	1566.4	1566.6	42	[HexNAc]3[Hex]4[Neu5Ac]1	Monoantennary complex	
20	1605.8	1578.2	+2	3154.4	1566.6	1566.6	—	—	—		
21	1605.8	1120.0	+3	3357.0	1769.2	1769.6	23	[HexNAc]4[Hex]4[Neu5Ac]1	Biantennary complex		
22	1605.8	1271.1	+3	3810.3	2222.5	2222.8	49	[HexNAc]4[Hex]5[Neu5Ac]2	Biantennary complex		
42	1525.7	1147.4	+3	3439.2	1931.5	1931.7	—	[HexNAc]4[Hex]5[Neu5Ac]1	Biantennary complex		
42	1525.7	1720.7	+2	3439.3	1931.6	1931.6	—	—	—		
35	1541.7*	1152.7	+3	3455.1	1931.4	1931.7	100	[HexNAc]4[Hex]5[Neu5Ac]1	Biantennary complex		

Table II. continued

Glycosylation site ID	Retention time (min)	Peptide theoretical MW <sup>a</sup>	Glycopeptides			Oligosaccharide			Relative peak intensity (%) <sup>b</sup>	Composition <sup>c</sup>	Deduced Type <sup>c</sup>
			<i>m/z</i>	Charge	Calculated MW <sup>a</sup>	Calculated MW <sup>a</sup>	Theoretical MW <sup>a</sup>				
G17	35	1541.7*	1728.6	+2	3455.2	1931.5	1769.4	1769.6	9	[HexNAc]4[Hex]4[Neu5Ac]1	Biantennary complex
	36	1541.7*	1098.7	+3	3293.1	1769.4	1769.5	1566.6	18	[HexNAc]3[Hex]4[Neu5Ac]1	Monoantennary complex
	36	1541.7*	1647.6	+2	3293.2	1769.5	2222.7	2222.8	19	[HexNAc]4[Hex]5[Neu5Ac]2	Biantennary complex
	36	1541.7*	1546.1	+2	3090.2	1566.5	1931.6	1931.7	100	[HexNAc]4[Hex]5[Neu5Ac]1	Biantennary complex
	38	1541.7*	1249.8	+3	3746.4	2222.7	1931.6	1931.7	100	[HexNAc]4[Hex]5[Neu5Ac]1	Biantennary complex
	51	1912.9	1276.5	+3	3826.5	1931.6	1931.7	2587.9	6	[HexNAc]5[Hex]6[Neu5Ac]2	Triantennary complex
	51	1912.9	1914.3	+2	3826.6	1931.7	2222.8	2222.8	39	[HexNAc]4[Hex]5[Neu5Ac]2	Biantennary complex
	54	1912.9	1495.3	+3	4482.9	2588.0	1931.7	1931.7	100	[HexNAc]4[Hex]5[Neu5Ac]1	Biantennary complex
G18	54	1912.9	1030.4	+4	4117.6	2222.7	1931.7	1931.7	100	[HexNAc]4[Hex]5[Neu5Ac]1	Biantennary complex
	54	1912.9	1373.5	+3	4117.5	2222.6	1931.7	1931.7	100	[HexNAc]4[Hex]5[Neu5Ac]1	Biantennary complex
	98	2836.5	1188.5	+4	4750.2	1931.7	1931.7	1769.6	10	[HexNAc]4[Hex]4[Neu5Ac]1	Biantennary complex
	98	2836.5	1584.4	+3	4750.1	1931.7	1769.6	2222.8	64	[HexNAc]4[Hex]5[Neu5Ac]2	Biantennary complex
	98	2836.5	1148.0	+4	4588.1	1769.6	2222.8	2222.8	64	[HexNAc]4[Hex]5[Neu5Ac]2	Biantennary complex
	102	2836.5	1009.3	+5	5041.3	2222.8	2223.7	2223.0	79	[HexNAc]4[Hex]5[Neu5Ac]1	Biantennary complex
	102	2836.5	1261.6	+4	5042.2	2223.7	1931.5	1931.7	100	[HexNAc]4[Hex]5[Neu5Ac]2	Biantennary complex
	103	2836.5	1681.5	+3	5041.5	2223.0	1931.5	2222.8	100	[HexNAc]4[Hex]5[Neu5Ac]2	Biantennary complex
G19	83	3155.5	1014.8	+5	5069.0	1931.5	1931.5	2222.8	79	[HexNAc]4[Hex]5[Neu5Ac]1	Biantennary complex
	86	3155.5	1073.1	+5	5360.5	2223.0	2223.0	2222.8	100	[HexNAc]4[Hex]5[Neu5Ac]2	Biantennary complex

<sup>a</sup>Monoisotopic mass value.<sup>b</sup>Relative peak intensity was calculated by comparing same charge state glycopeptide ions. The intensity of glycoform with maximum intensity at each glycosylation site was considered as 100%.<sup>c</sup>The oligosaccharide composition and type were deduced from its composition.

\*The glycopeptides including G16 were found to be oxidized at methionine residue.

When each product ion spectrum of the peptide ions in this LC/ESI MS/MS analysis was identified by the computer program Mascot, the sequence coverage of apoB100 was 38%. The ions,  $m/z$  1177.9 (+3) at 64 min, 1289.0 (+3) at 91 min, and 1053.2 (+3) at 84 min, were identified as TIHDLHLFIENIDFN<sup>2212</sup>KSGSSTASWIQNVDTK containing the potential *N*-glycosylation site Asn2212 (G7), SSVITLNTNAELFN<sup>3331</sup>QSDIVAHLSSSSVIDALQYK containing Asn3331 (G14), and DFHSEYIVSASN<sup>4404</sup>FTSQLSSQVEQLHR containing Asn4404 (G19), respectively (data not shown). These results indicate that some parts of these glycosylation sites were not glycosylated. There were many unexplained peptides and glycopeptides in the digest (data not shown). This may be due to the unexpected digestion or nonspecific cleavage of apolipoprotein B100 as well as the multiple isoforms of the proteins.

#### LC/ESI MS/MS analysis of chymotryptic digest of apoB100

To determine the carbohydrate at undetected glycosylation sites in the tryptic digest including Asn1341 and 1350 (G4 and G5), which belong to the same tryptic peptide, the chymotrypsin digest was analyzed by LC/ESI MS/MS using the same methodology. Figure 5A shows a TIC of the TOF MS scan for the full scan  $m/z$  700–2000. The collision energy was adjusted at 40–80 eV depending on the precursor ions. A TIC of the product ion scan and extracted ion chromatogram at  $m/z$  204.05–204.15 (HexNAc) are presented in Figure 5B and 5C, respectively.

Figure 6A shows the product ion spectrum of 768.4 (+2) at 14 min for the chymotryptic glycopeptide. The carbohydrate B<sup>+</sup> ions, y1 and b2 ions of peptide NW (residue 1341–1342), and peptide + GlcNAc ion were found in the product ion spectrum. The carbohydrate composition, [HexNAc]<sub>2</sub>[Hex]<sub>5</sub>, was deduced from the calculated carbohydrate molecular ion, 1234.6. Figure 6B shows the product ion spectrum of 1444.1 (+2) at 9 min for the glycopeptide. The carbohydrate B<sup>+</sup> ions, peptide and peptide + GlcNAc ions, and peptide fragment ions from the peptide SGGNT-STDHF (residue 1347–1356) were detected in the product ion spectrum. Carbohydrate molecular weight, 1882.8, was calculated and the oligosaccharide composition, [HexNAc]<sub>2</sub>[Hex]<sub>6</sub>, was deduced from the molecular weight. The peptide fragment ions were also detected in the product ion spectrum for the chymotryptic glycopeptides as tryptic glycopeptides. The peptide and peptide + GlcNAc ions were detected in product ion spectra. These ions helped us determine the peptide moiety of the glycopeptide ion.

Results of the site-specific analysis of glycosylation of the chymotryptic digest are summarized in Table III. The oligosaccharide heterogeneity at each of 13 *N*-glycosylation sites was determined by LC/ESI MS/MS from the chymotryptic digest of apoB100 (Table III).

#### Carbohydrate diversity of each site

Results for the tryptic digest and chymotryptic digest of apoB100 are listed in Table IV. The oligosaccharide composition and type were deduced based on the molecular weight and previously reported oligosaccharide structures of apoB100. No information on glycosylation at Asn7 and 2533 (G1 and 8) was obtained from the analysis of the

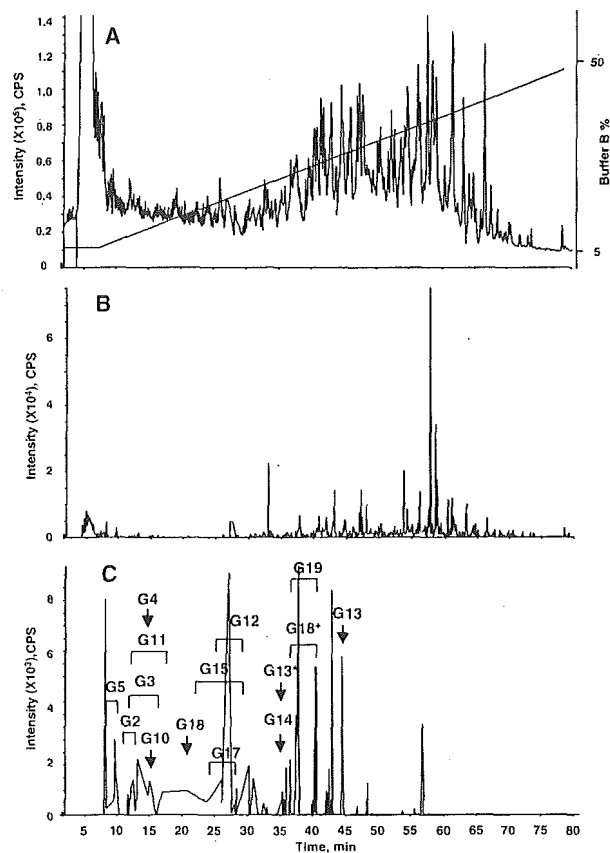


Fig. 5. LC/ESI MS/MS of chymotryptic digest of apolipoprotein B100. TIC of TOF MS scan for the full scan  $m/z$  700–2000 and the HPLC gradient are indicated (A). TIC of the product ion scan data-dependently acquired (B). Extract ion chromatogram at  $m/z$  204 of product ion spectra (C). Arrows and brackets denote glycopeptide fraction and *N*-glycosylation site ID. G13\* was found to be oxidized at a methionine residue. G18\* was found as missed cleaved glycopeptides.

tryptic or chymotryptic digest. When the tryptic digest of apoB100 was analyzed by LC/ESI MS/MS with the MS range  $m/z$  400–2000, the sequence coverage of apoB100 was 41% and tryptic peptides containing Asn7, 2212, 2533, or 2955 (G1, 7, 8, or 10) were detected (data not shown). Together with the result of LC/ESI MS/MS with the MS range  $m/z$  1000–2000, Asn7 and 2533 (G1 and 8) were not glycosylated or glycosylated only under detection sensitivity, and Asn2212, 2955, 3331, and 4404 (G7, 10, 14, and 19) were partially glycosylated. These findings indicate that 17 of 19 potential *N*-glycosylation sites in apoB100 were glycosylated.

The most heterogeneous oligosaccharides were found at Asn3384 (G15). Asn3384 possessed neutral or monosialylated hybrid and monoantennary complex type and mono- or disialylated biantennary complex type oligosaccharides as well as one high-mannose type oligosaccharide. Asn158, 1341, 1350, 3309, and 3331 (G2, 4, 5, 13, and 14) were occupied by high-mannose type oligosaccharides, whereas Asn956, 1496, 2212, 2752, 2955, 3074, 3197, 3438, 3868,



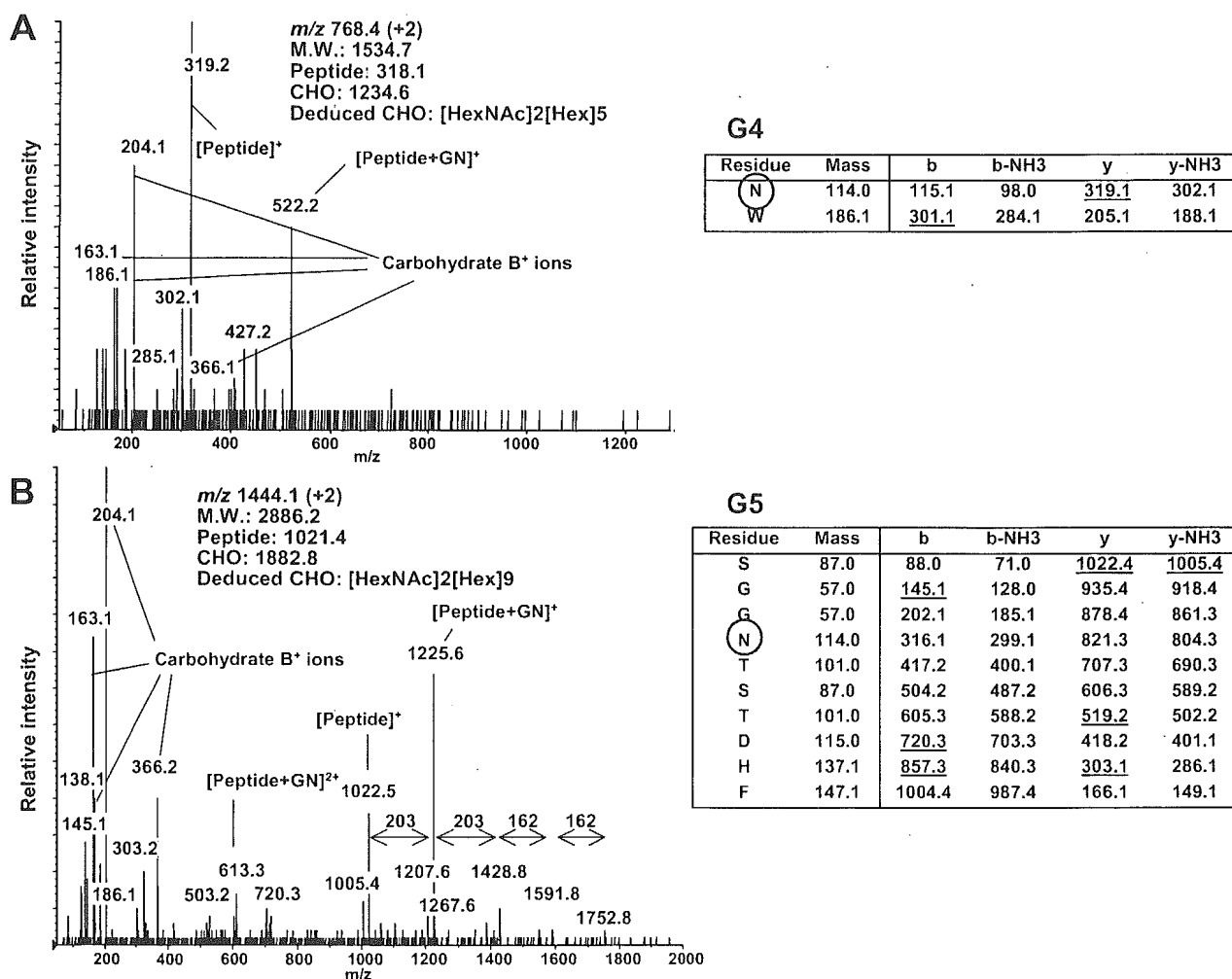


Fig. 6. Product ion spectra of the chymotryptic *N*-glycosylated peptides of apoB100. (A) Product ion spectrum of  $m/z$  768.4 (+2) at 14 min for the glycopeptide consisting of residues 1341–1342. Peptide b and y ions of the peptide NW were found. Table shows  $m/z$  of the proposed b- and y-series fragment ions, and the detected ions are underscored. (B) Product ion spectrum of  $m/z$  1444.1 (+2) at 9 min for the glycopeptide consisting of residues 1347–1356. Several ions are consistent with the b- and y-series fragment ions derived from the peptide SGGNTSTDHF. Table shows  $m/z$  of the proposed b- and y-series fragment ions, and the detected ions are underscored.

4210, and 4404 (G3, 6, 7, 9–12, and 16–19) were predominantly occupied by monosialylated or disialylated biantennary complex type oligosaccharides (Figure 7).

## Discussion

Although the role of the carbohydrate structures in LDL and/or apoB100 has been examined in several studies (Attie *et al.*, 1979; Filipovic *et al.*, 1979; Fujioka *et al.*, 2000; Orekhov *et al.*, 1989; Shireman and Fisher, 1979), it is still unknown. It is necessary to elucidate the diversity of the oligosaccharides at each *N*-glycosylation site. This is the first report on the characterization of *N*-linked oligosaccharides in apoB100 at each glycosylation site. The protein was initially carboxymethylated and digested with an enzyme

(trypsin or chymotrypsin), and then the complex mixtures of peptides and glycopeptides were subjected to LC/ESI MS/MS analysis. Product ion scan of each precursor ion was carried out in a data-dependent manner. The glycopeptide molecular ions were easily distinguished from peptide ions by the presence of carbohydrate-related oxonium ions, such as  $m/z$  204 (HexNAc), 186 (HexNAc-H<sub>2</sub>O), 168 (HexNAc-H<sub>2</sub>O), 366 (HexHexNAc), and others in product ion spectra. Furthermore, product ion spectra provided information for the elucidation of the amino acid sequence of the glycopeptides.

The oligosaccharide structure could be deduced based on the calculated molecular weight of the oligosaccharide moiety. The glycopeptide precursor ion was assigned using three strategies. (1) By comparing the product ions of the glycopeptide with the expected fragment ions derived from

Table III. Site-specific glycosylation analysis of the chymotryptic digest of apoB100 using LC/ESI-MS/MS

Glycosylation site ID	Retention time (min)	Peptide theoretical MW <sup>a</sup>	Glycopeptides		Oligosaccharide		Theoretical MW <sup>a</sup>	Relative peak intensity (%) <sup>b</sup>	Composition <sup>c</sup>	Deduced Type <sup>c</sup>
			m/z	Charge	Calculated MW <sup>a</sup>	Calculated MW <sup>a</sup>				
G1	—	560.3	—	—	—	—	—	—	—	—
G2	11	822.3	1344.5	+2	2687.0	1882.7	1882.6	4	[HexNAc]2[Hex]9	High mannose
	11	822.3	1263.5	+2	2525.0	1720.7	1720.6	7	[HexNAc]2[Hex]8	High mannose
	11	822.3	1182.5	+2	2363.0	1558.7	1558.5	15	[HexNAc]2[Hex]7	High mannose
	12	822.3	1101.4	+2	2200.8	1396.5	1396.5	12	[HexNAc]2[Hex]6	High mannose
	12	822.3	1020.4	+2	2038.8	1234.5	1234.4	100	[HexNAc]2[Hex]5	High mannose
G3	12	1088.4	1001.8	+3	3002.4	1932.0	1931.7	70	[HexNAc]4[Hex]5[Neu5Ac]1	Biantennary complex
	15	1088.4	1098.8	+3	3293.4	2223.0	2222.8	100	[HexNAc]4[Hex]5[Neu5Ac]2	Biantennary complex
G4	14	318.1	768.4	+2	1534.8	1234.7	1234.4	—	[HexNAc]2[Hex]5	High mannose
G5	9	1021.4	963.1	+3	2886.3	1882.9	1882.6	100	[HexNAc]2[Hex]9	High mannose
	9	1021.4	1444.1	+2	2886.2	1882.8	—	—	—	—
	9	1021.4	1363.1	+2	2724.2	1720.8	1720.6	40	[HexNAc]2[Hex]8	High mannose
	9 <sup>d</sup>	1021.4	1282.1	+2	2562.2	1558.8	1558.5	16	[HexNAc]2[Hex]7	High mannose
G6	—	469.2	—	—	—	—	—	—	—	—
G7	—	1023.5	—	—	—	—	—	—	—	—
G8	—	515.3	—	—	—	—	—	—	—	—
G9	—	2846.4	—	—	—	—	—	—	—	—
G10	15	279.1	829.0	+3	2484.1	2223.0	2222.8	—	[HexNAc]4[Hex]5[Neu5Ac]2	Biantennary complex
	15	279.1	1243.0	+2	2484.0	2222.9	—	—	—	—
G11	13	521.2	812.7	+3	2435.1	1931.9	1931.7	100	[HexNAc]4[Hex]5[Neu5Ac]1	Biantennary complex
	13	521.2	1218.5	+2	2435.0	1931.8	—	—	—	—
	16	521.2	909.8	+3	2726.3	2223.0	2222.8	52	[HexNAc]4[Hex]5[Neu5Ac]2	Biantennary complex
G12	28	878.5	1028.8	+3	3083.4	2222.9	2222.8	—	[HexNAc]4[Hex]5[Neu5Ac]2	Biantennary complex
G13	44	978.5	1341.6	+2	2681.2	1720.7	1720.6	31	[HexNAc]2[Hex]8	High mannose
	44	978.5	1260.6	+2	2519.1	1558.6	1558.5	50	[HexNAc]2[Hex]7	High mannose
	44	978.5	1179.5	+2	2357.1	1396.6	1396.5	100	[HexNAc]2[Hex]6	High mannose

Table III. continued

Glycosylation site ID	Retention time (min)	Peptide theoretical MW <sup>a</sup>	Glycopeptides		Oligosaccharide		Relative peak intensity (%) <sup>b</sup>	Composition <sup>c</sup>	Deduced Type <sup>e</sup>
			m/z	Charge	Calculated MW <sup>a</sup>	Theoretical MW <sup>a</sup>			
G14	44	978.5	1098.5	2	2195.0	1234.5	75	[HexNAc]2[Hex]5	High mannose
	35 <sup>d</sup>	995.5*	1349.6	+2	2697.1	1719.6	16	[HexNAc]2[Hex]8	High mannose
	35 <sup>d</sup>	995.5*	1268.5	+2	2535.0	1557.5	49	[HexNAc]2[Hex]7	High mannose
	35	995.5*	1187.5	+2	2373.0	1395.5	100	[HexNAc]2[Hex]6	High mannose
	35	995.5*	1106.5	+2	2211.0	1233.5	89	[HexNAc]2[Hex]5	High mannose
	35	995.5	954.4	+3	2860.3	1882.8	—	[HexNAc]2[Hex]9	High mannose
	35	995.5	1431.2	+2	2860.3	1882.8	—		
	24	1128.5	1173.5	+2	2345.0	1234.6	3	[HexNAc]2[Hex]5	High mannose
	24 <sup>d</sup>	1128.5	1275.0	+2	2548.0	1437.5	9	[HexNAc]3[Hex]5	Hybrid
	27	1128.5	1015.1	+3	3042.4	1931.9	100	[HexNAc]4[Hex]5[Neu5Ac]1	Biantennary complex
27	1128.5	947.4	+3	2839.3	1728.8	79	[HexNAc]3[Hex]5[Neu5Ac]1	Hybrid	
27	1128.5	893.4	+3	2677.3	1566.8	23	[HexNAc]3[Hex]4[Neu5Ac]1	Monoantennary complex	
30	1128.5	1112.2	+3	3333.5	2223.0	28	[HexNAc]4[Hex]5[Neu5Ac]2	Biantennary complex	
G16	—	530.2	—	—	—	—	—	—	—
G17	28	490.2	899.4	+3	2695.2	2223.0	—	[HexNAc]4[Hex]5[Neu5Ac]2	Biantennary complex
	28	490.2	1348.5	+2	2695.0	2222.8	—		
G18	21	1082.6	999.8	+3	2996.4	1931.8	100	[HexNAc]4[Hex]5[Neu5Ac]1	Biantennary complex
	25	1082.6	1096.8	+3	3287.4	2222.8	51	[HexNAc]4[Hex]5[Neu5Ac]2	Biantennary complex
	37	1229.6 <sup>f</sup>	786.9	+4	3143.5	1931.9	100	[HexNAc]4[Hex]5[Neu5Ac]1	Biantennary complex
	37	1229.6 <sup>f</sup>	1048.8	+3	3143.5	1931.8	—		
	38	1229.6 <sup>f</sup>	994.8	+3	2981.5	1769.9	14	[HexNAc]4[Hex]4[Neu5Ac]1	Biantennary complex
	40	1229.6 <sup>f</sup>	859.7	+4	3434.6	2223.0	67	[HexNAc]4[Hex]5[Neu5Ac]2	Biantennary complex
G19	40	1229.6 <sup>f</sup>	1145.9	+3	3434.6	2223.0	—		
	37	736.4	884.4	+3	2650.3	1931.9	100	[HexNAc]4[Hex]5[Neu5Ac]1	Biantennary complex
	37	736.4	1326.1	+2	2650.2	1931.8	—		
	40	736.4	981.4	+3	2941.2	2222.8	94	[HexNAc]4[Hex]5[Neu5Ac]2	Biantennary complex

<sup>a</sup>Monoisotopic mass value.<sup>b</sup>Relative peak intensity was calculated by comparing same charge state glycopeptide ions. The intensity of glycoform with maximum intensity at each glycosylation site was considered as 100%.<sup>c</sup>The oligosaccharide composition and type were deduced from its composition.<sup>d</sup>Product ion spectra were not acquired. These ions were considered as glycopeptides by the mass differences of 162(Hex) or 203(HexNAc) from the glycopeptides.<sup>e</sup>The glycopeptides including G13 were found to be oxidized at methionine residue.<sup>f</sup>Peptides of these glycopeptides including G18 were found as missed cleaved. The peptide sequence was considered as SKVHN<sup>210</sup>GSEILF.

Table IV. Summary of apoB100 oligosaccharide structure obtained from tryptic digest and chymotryptic digest

Glycosylation site ID	Deduced oligosaccharide composition <sup>a</sup>	Deduced oligosaccharide type <sup>a</sup>
G1	Not glycosylated	—
G2	[HexNAc]2[Hex]9	High mannose
G3	[HexNAc]4[Hex]3[Neu5Ac]1	Biantennary complex
G4	[HexNAc]2[Hex]5	High mannose
G5	[HexNAc]2[Hex]9	High mannose
G6	[HexNAc]2[Hex]5	High mannose
	[HexNAc]3[Hex]7[Neu5Ac]1	Hybrid
	[HexNAc]3[Hex]4[Neu5Ac]1	Monoantennary complex
	[HexNAc]4[Hex]4[Neu5Ac]1	Biantennary complex
	[HexNAc]4[Hex]5[Neu5Ac]2	Biantennary complex
G7	[HexNAc]4[Hex]5[Neu5Ac]1	Biantennary complex
	[HexNAc]4[Hex]5[Neu5Ac]2	Biantennary complex
G8	Not glycosylated	—
G9	[HexNAc]4[Hex]5[Neu5Ac]2	Biantennary complex
G10	[HexNAc]4[Hex]5[Neu5Ac]1	Biantennary complex
G11	[HexNAc]4[Hex]5[Neu5Ac]1	Biantennary complex
G12	[HexNAc]4[Hex]5[Neu5Ac]2	Biantennary complex
G13	[HexNAc]2[Hex]8	High mannose
G14	[HexNAc]2[Hex]9	High mannose
G15	[HexNAc]2[Hex]5	High mannose
	[HexNAc]3[Hex]6	Hybrid
	[HexNAc]3[Hex]4[Neu5Ac]1	Monoantennary complex
	[HexNAc]4[Hex]4	Biantennary complex
	[HexNAc]4[Hex]5[Neu5Ac]1[Fuc]1	Biantennary complex
G16	[HexNAc]3[Hex]4[Neu5Ac]1	Monoantennary complex
	[HexNAc]4[Hex]4[Neu5Ac]1	Biantennary complex
	[HexNAc]4[Hex]5[Neu5Ac]1	Biantennary complex
G17	[HexNAc]4[Hex]5[Neu5Ac]1	Biantennary complex
	[HexNAc]5[Hex]6[Neu5Ac]2	Triantennary complex
G18	[HexNAc]4[Hex]4[Neu5Ac]1	Biantennary complex
G19	[HexNAc]4[Hex]5[Neu5Ac]1	Biantennary complex

<sup>a</sup>The oligosaccharide structure was deduced from the molecular weight and previously reported oligosaccharide structures of apoB100.

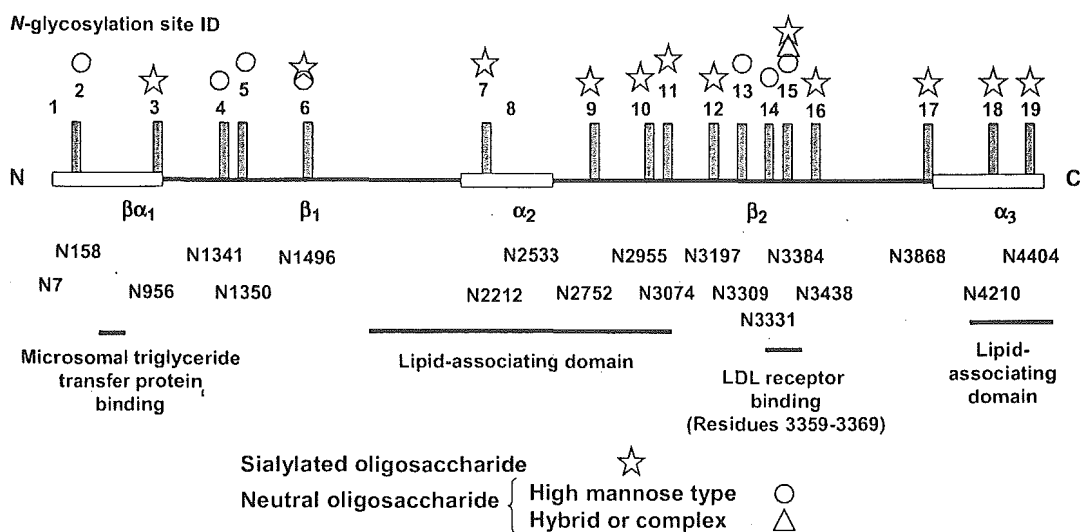


Fig. 7. *N*-glycosylation site of apoB100 and *N*-glycans at each site. *N*-glycosylation sites were shown on the pentapartite structure model, NH<sub>2</sub>-β<sub>1</sub>-β<sub>2</sub>-α<sub>2</sub>-β<sub>2</sub>-α<sub>3</sub>-COOH, previously reported (Segrest *et al.*, 1994). Circle, triangle, and star indicate high-mannose type oligosaccharides, neutral hybrid or neutral complex oligosaccharides, and mono- or disialylated oligosaccharides, respectively. High-mannose type oligosaccharides were found around the N-terminal and near the LDL-receptor binding site, and the other sites were attached by mono- or disialylated oligosaccharides. These oligosaccharide structures may reflect the local 3D structure of VLDL/LDL and may play a biological role.

the peptide containing the *N*-linked glycosylation site, we could directly deduce the peptide moiety. The molecular weight of the oligosaccharide moiety was calculated from the observed molecular weight of the glycopeptide and the theoretical molecular weight of the identified peptide. The carbohydrate composition and structure were deduced from the calculated molecular weight of the oligosaccharide. (2) There were relatively intense peaks of the peptide and peptide + GlcNAc ions in the glycopeptide product ion spectrum. Thus the *m/z* difference of 203 between fragment ions in the product ion spectrum could suggest the molecular weight of the peptide moiety. The peptide was determined from this suggested molecular weight and the molecular weight of the peptides containing the putative *N*-glycosylation site. The molecular weight of the carbohydrate was calculated, and the carbohydrate composition and structure were deduced. (3) Possible glycopeptide masses were calculated from the peptide masses containing the *N*-linked glycosylation site and possible *N*-linked oligosaccharide masses. The possible glycopeptide mass with the measured mass of the glycopeptide was identified. Assignment of peptide moiety was confirmed by the presence of the fragment ions derived from the peptide in the product ion spectrum.

The elution time as well as mass of a glycopeptide is also helpful to elucidate the oligosaccharide structure. The glycopeptides were eluted following reversed-phase high-performance LC based on the peptide and further separated based on the structure of the attached oligosaccharide (Kawasaki *et al.*, 2004). The glycopeptides having the same amino acid sequence were eluted in order of the number of Neu5Ac. Our results show that LC/ESI MS/MS with high sensitivity and high detection resolution is a powerful technique for the site-specific glycosylation analysis of glycoprotein.

Our study revealed that 17 of the 19 potential *N*-glycosylation sites in apoB100 were glycosylated, and the diversity of oligosaccharides at each of these *N*-glycosylation sites was determined. The deduced oligosaccharide structures in the present study were consistent with the structures previously identified in apoB100 (Garner *et al.*, 2001). Asn2212, which was reported to be unglycosylated (Yang *et al.*, 1989), could be glycosylated. The *N*-glycan structures and patterns are very different at each site. Asn158, 1341, 1350, 3309, and 3331 were occupied by high-mannose type oligosaccharides. The other sites except Asn1496 and 3384 (G6 and G15) were predominantly occupied by mono- or disialylated biantennary complex type oligosaccharides, and no neutral oligosaccharides were detected. These sialylated glycans may play an important biological role. Asn1496 and 3384 were occupied by high-mannose, hybrid, and complex type *N*-linked oligosaccharides. Hybrid-type oligosaccharides were found only at these two sites. The oligosaccharides at Asn 3384 are most heterogeneous, and at least 12 different oligosaccharide structures were present. Neutral complex type and neutral hybrid type oligosaccharides were detected only at this site. It is unlikely that this oligosaccharide heterogeneity is due to the fact that the apoB100 used in this study was extracted from the pooled serum of normolipidemic subjects, because no hybrid type oligosaccharides were detected except at Asn1496 and 3384 in this study, and it was reported that the diversity of the oligosaccharides of apoB100 was highly conserved among subjects (Garner *et al.*, 2001; Taniguchi *et al.*, 1989). It may be suggested that the diversity of the oligosaccharides at each glycosylation site was also conserved among subjects.

The relationship between sialylation and LDL-receptor binding has been examined. Desialylation of LDL increased the internalization of LDL by aortic smooth muscle cells

(Filipovic *et al.*, 1979), macrophage (Fujioka *et al.*, 2000) and aortic intimal cells (Orekhov *et al.*, 1989), but had no effect on degradation in hepatocytes (Attie *et al.*, 1979). These findings appear controversial. Asn3309, 3331, and 3384 are located near the LDL-receptor binding site in apoB100 (residues 3359–3369). Our data showed that these glycosylation sites were populated by high-mannose type (at Asn3309 and 3331) or a variety of oligosaccharides, including neutral or sialylated oligosaccharides (at Asn3384). These findings may indicate that sialic acid residues of apoB100 did not play a significant role in LDL-receptor binding and that desialylated LDL might be internalized by another mechanism. Shireman and Fisher (1979) reported that the removal of carbohydrate from LDL did not alter its binding to fibroblasts. Thus the carbohydrate moieties of LDL might not have a significant role in LDL-receptor binding.

The most interesting observation was that the most heterogeneous oligosaccharides were found at the *N*-glycosylation site (Asn3384) nearest to the LDL-receptor binding site. ApoB100 enwraps the VLDL and LDL particle. The C-terminal crosses over near the LDL-receptor binding site and inhibits binding of VLDL to the LDL receptor (Boren *et al.*, 1998). Conversion of VLDL to smaller LDL allows interaction with the LDL receptor. It is likely that the size of the VLDL/LDL particle could affect the 3D conformation around here. Thus the variety of oligosaccharide at Asn3384 may reflect the local 3D conformation of the VLDL particle and accessibility of trimming and glycosyl transferase enzymes.

The procedure described in this article provides an easy and efficient method for the identification of glycosylation sites and oligosaccharide heterogeneity of glycoproteins. Site-specific glycosylation analysis of apoB100 revealed that the diversity of oligosaccharide was distinct at each site. These data provide information to understand the role of oligosaccharides of apoB100 in LDL particles

## Materials and methods

### Materials

Acetonitrile, formic acid, chymotrypsin, and guanidine hydrochloride were from Wako Pure Chemicals (Osaka, Japan). Tosylphenylalanine chloromethane (TPCK)-treated trypsin was from Sigma (St. Louis, MO). Human apoB100 was purchased from MP Biomedicals (Irvine, CA). This product is derived from pooled human plasma, which is not particularly high-fat plasma. The water used was obtained from a Milli-Q water system (Millipore, Bedford, MA). All other reagents were of the highest quality available.

### Reduction and *S*-carboxymethylation of apoB100

ApoB100 (500 µg) was dissolved in 810 µl of 0.5 M Tris-HCl buffer (pH 8.5) that contained 8 M guanidine hydrochloride and 5 mM ethylenediamine tetra-acetic acid. After the addition of 6 µl 2-mercaptoethanol, the mixture was incubated for 2 h at 40°C. Then, 17 mg of monoiodoacetic acid was added, and the resulting mixture was incubated for 2 h at 40°C in the dark. The reaction mixture was applied to a PD-10 column (Amersham Pharmacia Biotech,

Uppsala, Sweden) to remove the reagents, and the eluate was lyophilized.

### Enzyme digestion of apoB100

Reduced and carboxymethylated apoB100 was redissolved in 500 µl 0.1 M Tris-HCl buffer (pH 8.0). Half of the reduced and carboxymethylated apoB100 was incubated with 0.02 µg/µl of TPCK-treated trypsin (1:50 w/w) for 2 h at 37°C and the rest was incubated with 0.04 µg/µl of chymotrypsin (1:25 w/w) for 72 h at 37°C. The enzyme digestions were stopped by storing at -20°C before analysis.

### High-performance LC of trypsin or chymotrypsin-digested apoB100

Tryptic digest (4 µg, about 8 pmol) and chymotryptic digest (2 µg, about 4 pmol) were analyzed by LC/ESI MS/MS. High-performance LC was performed on a Paradigm MS 4 equipped with a Magic C18 column (0.2 × 50 mm, Michrome BioResources, Auburn, CA). The eluents consisted of water containing 2% (v/v) acetonitrile and 0.1% (v/v) formic acid (pump A) and 90% acetonitrile and 0.1% formic acid (pump B). Trypsin- or chymotrypsin-digested samples of apoB100 were eluted with 5% B for 10 min, followed by a linear gradient from 5% to 70% of pump B in 130 min at a flow rate of 2 µl/min.

### ESI Q-TOF MS/MS

MS analyses were performed using a QSTAR Pulsar i quadrupole TOF mass spectrometer (AB/MDS Sciex, Toronto, Canada) equipped with a nano-electrospray ion source. The mass spectrometer was operated in the positive ion mode. The nanospray voltage was set at 2500 V. Mass spectra for MS analysis were acquired over *m/z* 1000–2000 and 700–2000 for tryptic and chymotryptic digests, respectively, and for MS/MS analysis, over *m/z* 100–2000. After every regular MS acquisition, MS/MS acquisition was performed against multiple charged ions. The molecular ions were selected by data-dependent acquiring in the quadrupole analyzer and fragmented in the hexapole collision cell. The collision energy was varied between 40 and 80 eV depending on the size and charge of the molecular ion. All signals were monoisotopically resolved. Accumulation time of spectra is 1.0 and 2.0 s for MS and MS/MS, respectively.

### Acknowledgments

We thank Dr. Nishimaki-Mogami for helpful suggestions. This study was supported by a grant-in-aid for Research on Health Sciences focusing on Drug Innovation from the Japan Health Sciences Foundation.

### Abbreviations

apoB100, apolipoprotein B100; ESI, electrospray ionization; LC, liquid chromatography; LDL, low-density lipoprotein; MS, mass spectrometry; TIC, total ion chromatogram; TOF, time of flight; TPCK, Tosylphenylalanine chloromethane; VLDL, very low-density lipoprotein.

## References

- Attie, A.D., Weinstein, D.B., Freeze, H.H., Pittman, R.C., and Steinberg, D. (1979) Unaltered catabolism of desialylated low-density lipoprotein in the pig and in cultured rat hepatocytes. *Biochem. J.*, **180**, 647-654.
- Boren, J., Lee, I., Zhu, W., Arnold, K., Taylor, S., and Innerarity, T.L. (1998) Identification of the low density lipoprotein receptor-binding site in apolipoprotein B100 and the modulation of its binding activity by the carboxyl terminus in familial defective apo-B100. *J. Clin. Invest.*, **101**, 1084-1093.
- Carr, S.A., Huddleston, M.J., and Bean, M.F. (1993) Selective identification and differentiation of N- and O-linked oligosaccharides in glycoproteins by liquid chromatography-mass spectrometry. *Protein Sci.*, **2**, 183-196.
- Chen, S.H., Yang, C.Y., Chen, P.F., Setzer, D., Tanimura, M., Li, W.H., Gotto, A.M. Jr, and Chan, L. (1986) The complete cDNA and amino acid sequence of human apolipoprotein B-100. *J. Biol. Chem.*, **261**, 12918-12921.
- Duffin, K.L., Welply, J.K., Huang, E., and Henion, J.D. (1992) Characterization of N-linked oligosaccharides by electrospray and tandem mass spectrometry. *Anal. Chem.*, **64**, 1440-1448.
- Filipovic, I., Schwarzmann, G., Mraz, W., Wiegandt, H., and Buddecke, E. (1979) Sialic-acid content of low-density lipoproteins controls their binding and uptake by cultured cells. *Eur. J. Biochem.*, **93**, 51-55.
- Fujioka, Y., Taniguchi, T., Ishikawa, Y., and Yokoyama, M. (2000) Significance of acidic sugar chains of apolipoprotein B-100 in cellular metabolism of low-density lipoproteins. *J. Lab. Clin. Med.*, **136**, 355-362.
- Garner, B., Harvey, D.J., Royle, L., Frischmann, M., Nigon, F., Chapman, M.J., and Rudd, P.M. (2001) Characterization of human apolipoprotein B100 oligosaccharides in LDL subfractions derived from normal and hyperlipidemic plasma: deficiency of alpha-N-acetylneuraminyl-lactosyl-ceramide in light and small dense LDL particles. *Glycobiology*, **11**, 791-802.
- Kawasaki, N., Ohta, M., Itoh, S., and Hayakawa, T. (2004) Analyses of glycopeptides and glycoproteins by liquid chromatography-mass spectrometry and liquid chromatography-tandem mass spectrometry. *Methods Mol. Biol.*, **251**, 263-274.
- Knott, T.J., Pease, R.J., Powell, L.M., Wallis, S.C., Rall, S.C. Jr, Innerarity, T.L., Blackhart, B., Taylor, W.H., Marcel, Y., Milne, R., and others. (1986) Complete protein sequence and identification of structural domains of human apolipoprotein B. *Nature*, **323**, 734-738.
- Law, S.W., Grant, S.M., Higuchi, K., Hospattankar, A., Lackner, K., Lee, N., and Brewer, H.B. Jr. (1986) Human liver apolipoprotein B-100 cDNA: complete nucleic acid and derived amino acid sequence. *Proc. Natl Acad. Sci. USA*, **83**, 8142-8146.
- Ling, V., Guzzetta, A.W., Canova-Davis, E., Stults, J.T., Hancock, W.S., Covey, T.R., and Shushan, B.I. (1991) Characterization of the tryptic map of recombinant DNA derived tissue plasminogen activator by high-performance liquid chromatography-electrospray ionization mass spectrometry. *Anal. Chem.*, **63**, 2909-2915.
- Orekhov, A.N., Tertov, V.V., Mukhin, D.N., and Mikhailenko, I.A. (1989) Modification of low density lipoprotein by desialylation causes lipid accumulation in cultured cells: discovery of desialylated lipoprotein with altered cellular metabolism in the blood of atherosclerotic patients. *Biochem. Biophys. Res. Commun.*, **162**, 206-211.
- Segrest, J.P., Jones, M.K., Mishra, V.K., Anantharamaiah, G.M., and Garber, D.W. (1994) ApoB-100 has a pentapartite structure composed of three amphipathic alpha-helical domains alternating with two amphipathic beta-strand domains. Detection by the computer program LOCATE. *Arterioscler Thromb.*, **14**, 1674-1685.
- Shireman, R.B. and Fisher, W.R. (1979) The absence of a role for the carbohydrate moiety in the binding of apolipoprotein B to the low density lipoprotein receptor. *Biochim. Biophys. Acta*, **572**, 537-540.
- Taniguchi, T., Ishikawa, Y., Tsunemitsu, M., and Fukuzaki, H. (1989) The structures of the asparagine-linked sugar chains of human apolipoprotein B-100. *Arch. Biochem. Biophys.*, **273**, 197-205.
- Vukmirica, J., Nishimaki-Mogami, T., Tran, K., Shan, J., McLeod, R.S., Yuan, J., and Yao, Z. (2002) The N-linked oligosaccharides at the amino terminus of human apoB are important for the assembly and secretion of VLDL. *J. Lipid. Res.*, **43**, 1496-1507.
- Yang, C.Y., Chen, S.H., Gianturco, S.H., Bradley, W.A., Sparrow, J.T., Tanimura, M., Li, W.H., Sparrow, D.A., DeLoof, H., Rosseneu, M., and others. (1986) Sequence, structure, receptor-binding domains and internal repeats of human apolipoprotein B-100. *Nature*, **323**, 738-742.
- Yang, C.Y., Gu, Z.W., Weng, S.A., Kim, T.W., Chen, S.H., Pownall, H.J., Sharp, P.M., Liu, S.W., Li, H.W., Gotto, A.M. Jr., and Chan, L. (1989) Structure of apolipoprotein B-100 of human low density lipoproteins. *Arteriosclerosis*, **9**, 96-108.



## Isotope tag method for quantitative analysis of carbohydrates by liquid chromatography–mass spectrometry

Jin Yuan<sup>1</sup>, Noritaka Hashii, Nana Kawasaki\*, Satsuki Itoh, Toru Kawanishi, Takao Hayakawa

*Division of Biological Chemistry and Biologicals, National Institute of Health Sciences, 1-18-1 Kamiyoga, Setagaya-ku, Tokyo 158-8501, Japan*

Available online 15 December 2004

### Abstract

We have previously demonstrated that liquid chromatography/mass spectrometry equipped with a graphitized carbon column (GCC-LC/MS) is useful for the structural analysis of carbohydrates in a glycoprotein. Here, we studied the monosaccharide composition analysis and quantitative oligosaccharide profiling by GCC-LC/MS. Monosaccharides were labeled with 2-aminopyridine and then separated and monitored by GCC-LC/MS in the selective ion mode. The use of tetradeuterium-labeled pyridylamino ( $d_4$ -PA) monosaccharides as internal standards, which were prepared by the tagging of standard monosaccharides with hexadeuterium-labeled 2-aminopyridine ( $d_6$ -AP), afforded a good linearity and reproducibility in ESIMS analysis. This method was successfully applied to the monosaccharide composition analysis of model glycoproteins, fetuin, and erythropoietin. For quantitative oligosaccharide profiling, oligosaccharides released from an analyte and a standard glycoprotein were tagged with  $d_0$ - and  $d_6$ -AP, respectively, and an equal amount of  $d_0$ - and  $d_4$ -PA oligosaccharides were coinjected into GCC-LC/MS. In this procedure, the oligosaccharides that existed in either analyte or a standard glycoprotein appeared as single ions, and the oligosaccharides that existed in both analyte and a standard glycoprotein were detected as paired ions. The relative amount of analyte oligosaccharides could be determined on the basis of the analyte/internal standard ion-pair intensity ratio. The quantitative oligosaccharide profiling enabled us to make a quantitative and qualitative comparison of glycosylation between the analyte and standard glycoproteins. The isotope tag method can be applicable for quality control and comparability assessment of glycoprotein products as well as the analysis of glycan alteration in some diseases.

© 2004 Elsevier B.V. All rights reserved.

**Keywords:** Monosaccharides; Oligosaccharides; Pyridylation; Isotope tag

### 1. Introduction

A variety of recombinant glycoproteins and modified glycoproteins are developed as medical agents, and most of them exist in heterogeneous forms because of the various combinations of oligosaccharides. Alteration of glycosylation is

known to affect the biological activity, mobilization, and biophysical properties of glycoproteins [1], so assessments of their carbohydrate structure and heterogeneity are essential in many stages of development and quality control of glycoprotein products. Since glycosylation varies in response to changes in the manufacturing condition, monosaccharide composition analysis and/or oligosaccharide profiling are needed for the characterization and as a test for constancy and comparability assessments of glycosylation [2]. Several analytical procedures using HPLC have been reported for oligosaccharide profiling and structural analysis of carbohydrates [3–5]. The oligosaccharide profiling using liquid chromatography/mass spectrometry (LC/MS) is especially known to provide structural information from their chromatographic behavior and molecular mass [6–8]. We have developed mass spectrometric oligosaccharide profiling using a graphitized carbon column (GCC), which can separate

**Abbreviations:** AP, 2-aminopyridine;  $d_0$ , non-deuterium-labeled;  $d_4$ , tetradeuterium-labeled;  $d_6$ , hexadeuterium-labeled; Fuc, fucose; Gal, galactose; GalN, galactosamine; GalNAc, *N*-acetylgalactosamine; GCC, graphitized carbon column; Glc, glucose; GlcN, glucosamine; GlcNAc, *N*-acetylglucosamine; Man, mannose; PA, pyridylamino; R.S.D., relative standard deviation; SIM, selected ion mode; TFA, trifluoroacetic acid; TIC, total ion chromatogram

\* Corresponding author. Tel.: +81 3 3700 1141; fax: +81 3 3707 6950.

E-mail address: [nana@nih.go.jp](mailto:nana@nih.go.jp) (N. Kawasaki).

<sup>1</sup> Present address: Chengdu Institute of Biological Products, 610063, Chengdu Wai Dong Bao Jiang Qiao, Sichuan Province, China.



oligosaccharides based on subtle differences in branch, position, and linkage with volatile solution [9,10]. This method enables us to distinguish the glycosylation among some glycoprotein products produced in different cells [11].

A use of internal standards is known to improve the precision and linearity in quantitative analyses. Isotopic analogs of the analytes are currently the preferred internal standards for quantification by mass spectrometry (MS) procedures. For instance, Gygi et al. [12] demonstrated the approach for the accurate quantification of the proteins within complex mixture using isotope-coded affinity tags (ICATs). The use of the isotope-labeled carbohydrates as internal standards can make it possible to quantify the carbohydrates by LC/MS. Reductive pyridylation is frequently used for the tagging of carbohydrates in HPLC analysis [13,14]. This derivatization is known to afford higher sensitivity in MS analysis [15], and PA oligosaccharides were reported to be separated by GCC [16]. Here, we study quantitative analysis of carbohydrates using tetradeuterium-labeled pyridylamino ( $d_4$ -PA) carbohydrates as internal standards. First, we study the monosaccharide composition analysis by using  $d_4$ -PA monosaccharides as internal standards. Next, the isotope tag method is used for the quantitative oligosaccharide profiling using recombinant human chorionic gonadotropin (rhCG) and human chorionic gonadotropin (hCG) as an analyte and standard glycoproteins, respectively.

## 2. Materials and methods

### 2.1. Materials

All monosaccharide standards were purchased from Seikagaku-kogyo (Tokyo, Japan). The pyridylation apparatus (PALSTATION), reagents for the pyridylation reaction, and PA monosaccharide standards were available from TaKaRa Biomedicals (Otsu, Japan). The hexadeuterium-labeled 2-aminopyridine ( $d_6$ -AP) was purchased from Wako (Osaka, Japan). Human chorionic gonadotropin (hCG) and recombinant hCG (rhCG) were bought from Sigma (St. Louis, MO, USA). *N*-glycosidase F was purchased from Roche Diagnostics. All other chemicals and reagents were of analytical grade and were commercially available.

### 2.2. Pyridylation of monosaccharides

For the pyridylation of amino sugars, free amino groups of monosaccharides (GlcN, GalN, 1–1000 pmol) were acetylated by incubation in 50  $\mu$ l of methanol/pyridine/distilled water (30/15/10, v/v/v) with 2  $\mu$ l of acetic anhydride for 30 min at room temperature. The mixture was dried using a vacuum centrifuge evaporator without heating. Acetic acid (50  $\mu$ l), methanol (60  $\mu$ l), and 10  $\mu$ l of coupling reagent prepared by mixing 100 mg of AP was added to monosaccharides (Fuc, Gal, Glc, Man, GlcNAc, GalNAc, 1–1000 pmol). The mixture was heated at 90 °C for 20 min by PALSTATION, and the excess reagents were removed by evaporation under a stream of nitrogen gas at 60 °C for 20 min. Then 10  $\mu$ l of a reducing reagent, prepared just before use by mixing 6 mg of borane–dimethylamine complex and 100  $\mu$ l of acetic acid, was added, and the mixture was heated at 90 °C for 35 min. The reaction mixture was dried three times under a stream of nitrogen gas at 50 °C for 10 min. The residue was dissolved in water for LC/MS analysis. For the preparation of isotope analogs, the tetradeuterium-labeled PA ( $d_4$ -PA) monosaccharide,  $d_0$ -AP was just replaced by  $d_6$ -AP (Fig. 1).

### 2.3. Monosaccharide composition analysis of a glycoprotein

A glycoprotein (25 pmol) was placed in a hydrolysis tube fitted with a Teflon-lined screw cap. Fifty microliters of 2 M HCl–2 M trifluoroacetic acid (TFA) was added to the sample, which was then heated at 100 °C for 6 h. Simultaneously, a set of monosaccharide standards, 100 pmol of Gal, Man, Glc, Fuc, GlcN, and GalN, was treated identically as the analytes. The solution obtained was freeze-dried. The monosaccharides obtained from the analyte glycoproteins and standard monosaccharides were tagged with non-deuterium-labeled 2-aminopyridine ( $d_0$ -AP) and  $d_6$ -AP, respectively. Each tagged oligosaccharide mixture was dissolved into purified water, and a mixture of  $d_0$ - and  $d_4$ -PA monosaccharides was injected into the GCC-LC/MS.

### 2.4. Preparation of *N*-linked oligosaccharides

*N*-linked oligosaccharides were released from hCG as described previously [17]. Briefly, hCG and rhCG (100  $\mu$ g)

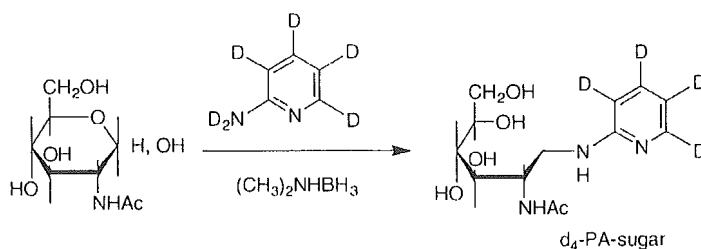


Fig. 1. Synthesis of  $d_4$ -PA monosaccharide internal standard.

were dissolved in 360  $\mu$ l of 0.5 M Tris-HCl buffer (pH 8.6), containing 8 M guanidine hydrochloride and 5 mM ethylenediaminetetra-acetic acid (EDTA). After an addition of 2.6  $\mu$ l of 2-mercaptoethanol, the mixture was allowed to stand at room temperature for 2 h. To this solution, 7.56 mg of monoiodoacetic acid was added, and the resulting mixture was incubated at room temperature for 2 h in the dark. The reaction mixture was applied to a PD-10 column (Amershambioscience, Uppsala, Sweden) to remove the reagents, and the eluate was lyophilized.

Carboxymethylated hCG and rhCG were dissolved in 100  $\mu$ l of 0.1 M sodium phosphate buffer, pH 7.2, and incubated with 5 units of PNGase F at 37 °C for 2 days. Protein was precipitated with 340  $\mu$ l of cold ethanol, and the supernatant was dried.

### 2.5. Pyridylation of oligosaccharides from hCG

To the lyophilized oligosaccharides released from rhCG we added 10  $\mu$ l of coupling reagent prepared by mixing 300 mg of  $d_0$ -AP, and 100  $\mu$ l of acetic acid, and the reaction mixture was heated at 90 °C for 60 min. Then, 10  $\mu$ l of a reducing reagent, prepared just before use by mixing 20 mg of borane-dimethylamine complex and 100  $\mu$ l of acetic acid, was added, and the mixture was heated at 80 °C for 60 min. The reaction mixture was dried three times under a stream of nitrogen gas at 60 °C for 10 min. The residue was dissolved in water for LC/MS analysis. For the preparation of the tetradeuterium-labeled ( $d_4$ )-PA oligosac-

charide isotope analogs,  $d_0$ -AP was just replaced by  $d_6$ -2-aminopyridine.

### 2.6. LC/MS analysis

LC was carried out using a Magic 2002 HPLC system (Michrom BioResources Inc., Auburn, CA, USA) using a Hypercarb column (0.2 mm  $\times$  150 mm, Thermoelectron, San Jose, CA, USA). The flow rate was set at 2–3  $\mu$ l/min through a splitter system. The mobile phases were 5 mM ammonium acetate (pH 8.5) with 2% of acetonitrile (pump A) and 80% of acetonitrile (pump B). A gradient of 10–35% of B in 60 min was used for the monosaccharide analysis. For oligosaccharide profiling, we used a gradient of 5–20% of B in 20 min, 20–70% of B in 15 min, and 70–95% of B in 5 min. The mass spectrometer used was a TSQ 7000 (Thermoelectron) equipped with a nanoelectrospray ion source (AMR Inc., Tokyo, Japan). The ESI voltage was set to 2000 V (positive ion mode) or 1500 V (negative ion mode), and the capillary temperature was 175 °C.

## 3. Results

### 3.1. Monosaccharide composition analysis using the isotope tag method

First, we examined the possibility of the isotope-tag method for the monosaccharide composition analysis of gly-

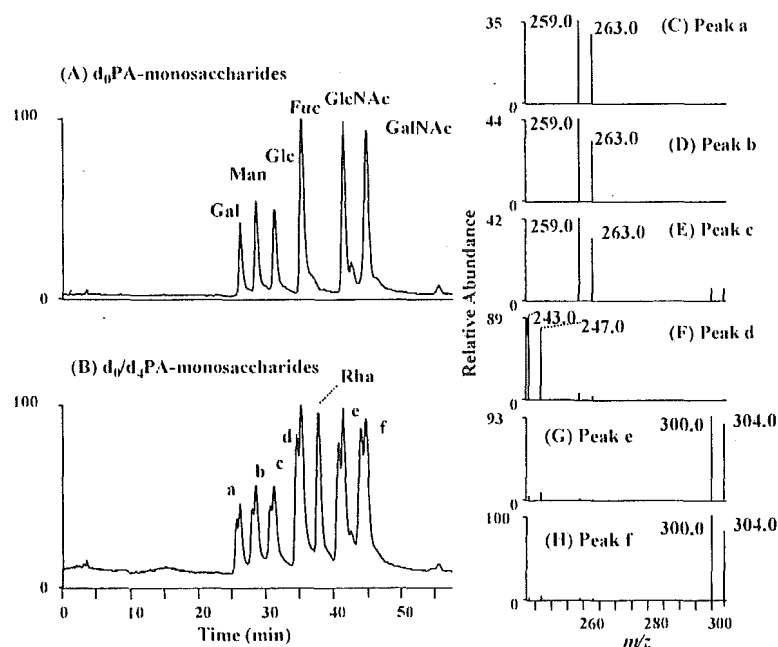


Fig. 2. (A) Extracted ion chromatogram (set  $m/z$  values, 243, 259, and 300) of  $d_0$ -PA monosaccharides (1 pmol Gal, Man, Glc, Fuc, GlcNAc, and GalNAc). (B) Extracted ion chromatogram (set  $m/z$  values, 243, 247, 259, 263, 300, and 304) of a mixture of  $d_0$ - and  $d_4$ -PA monosaccharides (1 pmol Gal, Man, Glc, Fuc, Rham, GlcNAc and GalNAc). (C) Mass spectra of peaks a (C), b (D), c (E), d (F), e (G), and f (H).

coproteins. An equal molar of each  $d_0$ -PA monosaccharide (Gal, Man, Glc, Fuc, GlcNAc, and GalNAc, 1 pmol each) was analyzed by GCC-LC/MS in the positive ion mode. The ions monitored were  $m/z$  259 (for  $d_0$ -PA-Gal,  $d_0$ -PA-Man, and  $d_0$ -PA-Glc),  $m/z$  243 ( $d_0$ -PA-Fuc), and  $m/z$  300 ( $d_0$ -PA-GlcNAc and  $d_0$ -PA-GalNAc). Fig. 2A shows the mass chromatogram of the  $d_0$ -PA monosaccharides. All six  $d_0$ -PA monosaccharides were retained and separated by GCC. The detection limit at a signal-to-noise ratio of 3 was 45 fmol.

The  $d_4$ -PA monosaccharides were prepared as internal standards by tagging of standard monosaccharides with  $d_6$ -AP and combined with  $d_0$ -PA monosaccharides. Fig. 2B shows the chromatogram of a mixture of  $d_0$ -,  $d_4$ -PA monosaccharides and PA-labeled Rhamnose, which is frequently used as an internal standard in the monosaccharide composition analysis. Paired ions with a difference of  $m/z$  4 were detected in the mass spectra of peaks a–f (Fig. 2C–H). When 0.5 pmol  $d_0$ -PA monosaccharides were determined in the presence of  $d_4$ -PA monosaccharides or Rhamnose by GCC-LC/MS, the relative standard deviation ( $n = 5$ ) was 1.8–4.8% or 5.6–8.3%, respectively.

To assess the linearity and reproducibility of the whole procedure, including reacylation, pyridylation, the removal of excess derivatization reagents, and GCC-LC/MS, we tagged different amounts of monosaccharides (Gal, Man, Glc, Fuc, GlcN, and GalN, 1–1000 pmol) with  $d_0$ -AP, and  $d_4$ -PA monosaccharides (4 or 20 pmol) were added to the  $d_0$ -PA monosaccharides (1–10 pmol or 10–1000 pmol, respectively). The whole process of the isotope tag method was found to be linear for all six monosaccharides over the tested range of 1–1000 pmol (Fig. 3). The accuracy of this method was approximately 80–100% (Fig. 3), and the relative standard deviations (%R.S.D.) were less than 7.2% for all monosaccharides (based on the peak area ratio of monosaccharides from five samples).

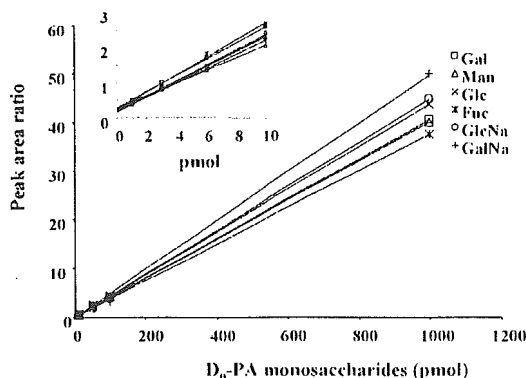


Fig. 3. Linearity on the isotope-tag method for monosaccharide quantification. For the internal standards, 1000 pmol monosaccharides were derivatized to  $d_4$ -PA monosaccharides. Different amounts of monosaccharides were derivatized to  $d_0$ -PA monosaccharides and co-injected with 4 pmol (A) or 20 pmol (B) internal standards into GCC-LC/MS.

We used this method for the monosaccharide composition analysis of fetuin and erythropoietin. Accuracy in the monosaccharide composition analysis of a glycoprotein relies on the condition of hydrolysis. Fan et al. [18] studied the hydrolysis of N-linked oligosaccharides and recommended 4 h with 2 M TFA at 100 °C for neutral sugars, and 6 h with 4 M HCl at 100 °C for amino sugars. While these hydrolysis conditions result in the complete release of neutral and amino sugars with no degradation, it takes two hydrolyses for a single sample. To quantify both neutral and amino sugars in glycoproteins in the same run, fetuin and erythropoietin (25 pmol) were heated in 2 M HCl-2M TFA at 100 °C for 6 h [19], and a set of monosaccharide standards, 100 pmol of Gal, Man, Glc, Fuc, GlcN, and GalN, was treated identically as the analyte glycoproteins. After hydrolysis, the analyte and standard monosaccharides were tagged with  $d_0$ - and  $d_6$ -AP, respectively. Fig. 4A and E show the mass chromatogram of monosaccharides prepared from fetuin and erythropoietin in the presence of  $d_4$ -PA monosaccharides, respectively.

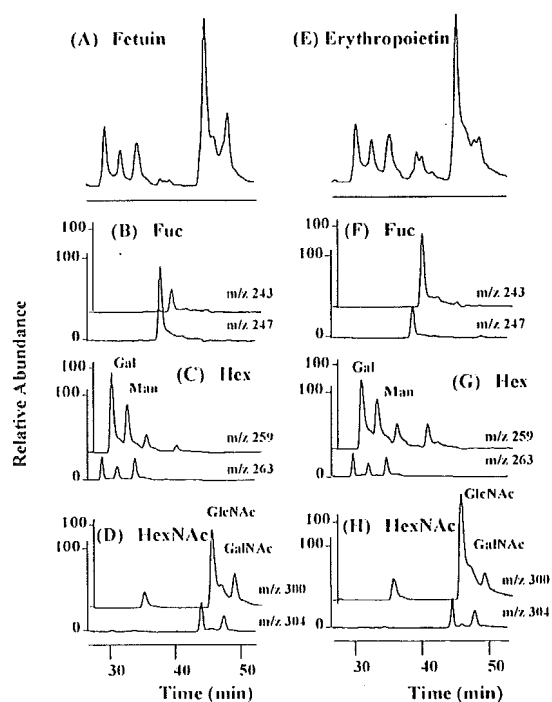


Fig. 4. Monosaccharide composition analysis of glycoproteins. Extracted ion chromatograms of  $d_0$ -PA monosaccharides from fetuin and  $d_4$ -PA standard monosaccharides (set  $m/z$  values, 243, 247, 259, 263, 300, and 304) (A),  $d_0$ -PA Fuc from fetuin and  $d_4$ -PA standard Fuc (set  $m/z$  values, 243 and 247) (B),  $d_0$ -PA Hex from fetuin and  $d_4$ -PA standard Hex (set  $m/z$  values, 259 and 263) (C), and  $d_0$ -PA HexNAc from fetuin and  $d_4$ -PA standard HexNAc and (set  $m/z$  values, 300 and 304) (D). Extracted ion chromatograms of  $d_0$ -PA monosaccharides from erythropoietin and  $d_4$ -PA standard monosaccharides and (set  $m/z$  values, 243, 247, 259, 263, 300, and 304) (E),  $d_0$ -PA Fuc from erythropoietin and  $d_4$ -PA standard Fuc (set  $m/z$  values, 243 and 247) (F),  $d_0$ -PA Hex from erythropoietin and  $d_4$ -PA standard Hex (set  $m/z$  values, 259 and 263) (G), and  $d_0$ -PA HexNAc from erythropoietin and  $d_4$ -PA standard HexNAc (set  $m/z$  values, 300 and 304) (H).

Table 1  
Monosaccharide composition analysis by isotope-tag method

Glycoprotein	Monosaccharide	mol/mol <sup>a</sup>	mol/mol
Fetuin	Fuc	0.3	0 [20]
	Gal	10.4	12
	Man	7.6	9
	GlcNAc	14.7	15
	GalNAc	3.4	3
Erythropoietin	Fuc	3.4	4.1 [21]
	Gal	12.8	13.8
	Man	8.1	8.7
	GlcNAc	15.6	17.2
	GalNAc	1.5	0.9

<sup>a</sup> Values were expressed as mol detected in 1 mol glycoprotein.

Fig. 4B, and F show the mass chromatograms of d<sub>0</sub>- and d<sub>4</sub>-PA fucose, Fig. 4C and G indicate those of d<sub>0</sub>- and d<sub>4</sub>-PA hexose, and Fig. 4D and H show those of d<sub>0</sub>- and d<sub>4</sub>-PA HexNAc. The monosaccharide compositions of fetuin and erythropoietin calculated from the peak area ratios (d<sub>0</sub>-PA/d<sub>4</sub>-PA monosaccharides) were in good agreement with the reported values (Table 1) [20,21]. By heating the standard monosaccharides simultaneously the decomposition of monosaccharides during hydrolysis can be corrected, and a use of isotope analogs as the internal standards can reduce deviation in ESIMS analysis.

### 3.2. Quantitative oligosaccharide profiling using the isotope tag method

Next, we explored the capability of the isotope-tag method for the quantitative oligosaccharide profiling. When d<sub>0</sub>-PA oligosaccharides prepared from an analyte glycoprotein are analyzed with an equal part of d<sub>4</sub>-PA oligosaccharides prepared from a standard glycoprotein, oligosaccharides which link to both the analyte and the standard glycoproteins are expected to appear as paired ions with a difference of 4 Da, and the individual oligosaccharides in the analyte glycoprotein can be quantified based on the analyte/internal standard ion-pair intensity ratio. On the other hand, any oligosaccharides that link to either the analyte or the standard glycoprotein ought to be detected as single ions. Oligosaccharides released from rhCG and hCG were tagged with d<sub>0</sub>- and d<sub>6</sub>-AP, respectively, and the tagged oligosaccharides were analyzed by GCC-LC/MS in both positive and negative ion modes.

Fig. 5A and B show the mass spectra of the peak which was detected at 21.5 min in the positive and the negative ion mode, respectively. In the positive ion mode, ions at *m/z* 863.0, 1359.4 and 1197.2 were detected (Fig. 5A), and they can be assigned to d<sub>4</sub>-PA [Hex]<sub>5</sub>[HexNAc]<sub>4</sub><sup>2+</sup> (an asialobiantennary oligosaccharide), d<sub>4</sub>-PA[Hex]<sub>3</sub>[HexNAc]<sub>4</sub><sup>+</sup> (a fragment of the asialobiantennary form) and d<sub>4</sub>-PA[Hex]<sub>4</sub>[HexNAc]<sub>4</sub><sup>+</sup> (a fragment of the asialobiantennary form), respectively. In contrast, only an ion at *m/z* 860.9 (d<sub>4</sub>-PA[Hex]<sub>5</sub>[HexNAc]<sub>4</sub><sup>2-</sup>, asialobiantennary oligosaccharide) was detected in the negative ion mode (Fig. 5B). This result suggests that mass spectra

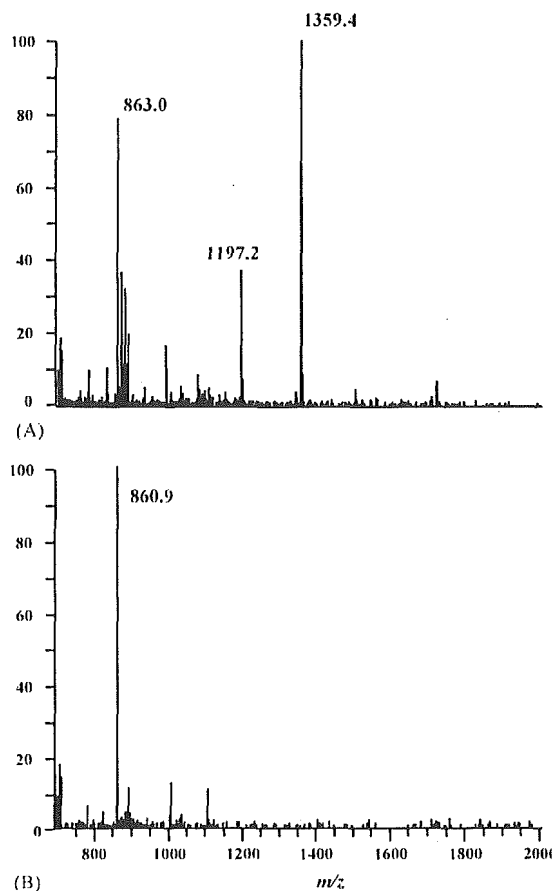


Fig. 5. Mass spectra of d<sub>4</sub>-PA oligosaccharide. D<sub>4</sub>-PA oligosaccharide eluted at 21.5 min from GCC was analyzed by ESIMS in the positive ion mode (A) and negative ion mode (B).

of PA oligosaccharides become complicated due to fragmentation in the positive ion mode, while only molecular ions can be detected in the negative ion mode. Therefore, ESI analysis in the negative ion mode was chosen for the PA oligosaccharide profiling.

Fig. 6A and B show the TIC of a mixture of equal parts of d<sub>0</sub>-PA oligosaccharides prepared from rhCG and d<sub>4</sub>-PA oligosaccharides from hCG, and its two-dimensional display (retention time versus *m/z*), respectively. The carbohydrate structures, which can be deduced from *m/z* values, are indicated in Table 2. Paired ions at *m/z* 757.5, 759.5 were observed in the mass spectrum of peak a1. Based on carbohydrate composition [Hex]<sub>5</sub>[HexNAc]<sub>3</sub>, it can be assigned to a hybrid type oligosaccharide. Likewise, peak 11, 12, 14, 15, p1, p2, and p4 consisted of paired ions and can be assigned to monosialylated (11, 12, 14, 15) and disialylated (p1, p2) biantennary oligosaccharide without Fuc. Fig. 7 shows TIC of d<sub>0</sub>- and d<sub>4</sub>-PA oligosaccharides (A), extracted ion chromatograms of d<sub>0</sub>-PA (B), d<sub>4</sub>-PA (C), and d<sub>0</sub>- and d<sub>4</sub>-PA monosialylated biantennary form (D). The mass spectra of peaks 11–15 are shown in Fig. 7E–I. Peak 13 was not observed in Fig. 7D and only